General Disclaimer

One or more of the Following Statements may affect this Document

- This document has been reproduced from the best copy furnished by the organizational source. It is being released in the interest of making available as much information as possible.

- This document may contain data, which exceeds the sheet parameters. It was furnished in this condition by the organizational source and is the best copy available.

- This document may contain tone-on-tone or color graphs, charts and/or pictures, which have been reproduced in black and white.

- This document is paginated as submitted by the original source.

- Portions of this document are not fully legible due to the historical nature of some of the material. However, it is the best reproduction available from the original submission.

NASA CR 168018

Department of Aerospace Engineering
and Applied Mechanics
University of Cincinnati

ENVIRONMENTAL SOLID PARTICLE EFFECTS ON COMPRESSOR CASCADE PERFORMANCE

BY

W. TABAKOFF AND C. BALAN

Supported by:

NATIONAL AERONAUTICS AND SPACE ADMINISTRATION

Lewis Research Center

Grant No. NSG 3218

October 1982

NASA CR 168018

ENVIRONMENTAL SOLID PARTICLE EFFECTS ON COMPRESSOR CASCADE PERFORMANCE

by

W. Tabakoff and C. Balan

Department of Aerospace Engineering and Applied Mechanics
University of Cincinnati
Cincinnati, Ohio 45221

Supported by:

NATIONAL AERONAUTICS AND SPACE ADMINISTRATION

Lewis Research Center

Grant No. NSG 3218

October 1982

1. Report No.	2. Government Accession No.	3. Recipient's Catalog No.
NASA CR 168018		

4. Title and Subtitle	5. Report Date
ENVIRONMENTAL SOLID PARTICLE EFFECTS ON COMPRESSOR CASCADE PERFORMANCE	OCTOBER 1982
	6. Performing Organization Code
7. Author(s)	8. Performing Organization Report No.
W. TABAKOFF and C. BALAN	
	10. Work Unit No.
9. Performing Organization Name and Address	11. Contract or Grant No.
DEPT. OF AEROSPACE ENGINEERING & APPLIED MECHANICS UNIVERISTY OF CINCINNATI CINCINNATI, OHIO 45221	NSG 3218
	13. Type of Report and Period Covered
12. Sponsoring Agency Name and Address	Contractor Report
NATIONAL AERONAUTICS AND SPACE ADMINISTRATION LEWIS RESEARCH CENTER CLEVELAND, OHIO 44135	14. Sponsoring Agency Code

15. Supplementary Notes

Project Manager, Mr. Robert Stubbs, Mail Stop 5-9,
NASA Lewis Research Center, Cleveland, Ohio 44135.

16. Abstract

Experimental and theoretical investigations of the effect of suspended solid particles on the performance of the compressor cascade is presented. The experimental investigation was carried out in a specially built cascade tunnel, using quartz sand particles. The cascades were made of NACA 65(10)10 airfoils. Three cascades were tested, one accelerating cascade and two diffusing cascades.

The theoretical analysis assumes inviscid and incompressible two dimensional flow. The momentum exchange between the fluid and the particle is accounted for by the interphase force terms in the fluid momentum equation. The modified fluid phase momentum equations and the continuity equation are reduced to the conventional stream function-vorticity formulation. The method treats the fluid phase in the Eulerian system and the particle phase in Lagrangian system. In addition, the inelastic collision between the particle and the blade surfaces are accounted for in the computation. The equations were solved numerically in a shifting coordinate system which enables space marching solution of the vorticity equation.

The experimental results indicate a small increase in the blade surface static pressures, while the theoretical results indicate a small decrease. The theoretical analysis, also predicts the loss in total pressure associated with the particulate flow through the cascade.

17. Key Words (Suggested by Author(s))	18. Distribution Statement
Particulate Flow Turbomachinery	Unclassified - unlimited STAR Category 02

19. Security Classif. (of this report)	20. Security Classif. (of this page)	21. No. of Pages	22. Price*
UNCLASSIFIED	UNCLASSIFIED	59	

* For sale by the National Technical Information Service, Springfield, Virginia 22161

TABLE OF CONTENTS

LIST OF FIGURES

SUMMARY

Experimental and theoretical investigations of the effect of suspended solid particles on the performance of the compressor cascade is presented. The experimental investigation was carried out in a specially built cascade tunnel, using quartz sand particles. The cascades were made of NACA 65(10)10 airfoils. Three cascades were tested, one accelerating cascade and two diffusing cascades.

The theoretical analysis assumes inviscid and incompressible two dimensional flow. The momentum exchange between the fluid and the particle is accounted for by the interphase force terms in the fluid momentum equation. The modified fluid phase momentum equations and the continuity equation are reduced to the conventional stream function-vorticity formulation. The method treats the fluid phase in the Eulerian system and the particle phase in Lagrangian system. In addition, the inelastic collision between the particle and the blade surfaces are accounted for in the computation. The equations were solved numerically in a shifting coordinate system, which enables space marching solution of the vorticity equation.

The experimental results indicate a small increase in the blade surface static pressures, while the theoretical results indicate a small decrease. The theoretical analysis, also predicts the loss in total pressure associated with the particulate flow through the cascade.

INTRODUCTION

The ingestion of sand in aircraft engines can cause serious damage to the engine in terms of sudden loss of power due to the momentum exchange between the fluid and the solid particles. This is only a temporary phenomenon and the effect lasts only for the duration of the sand ingestion. In addition to this temporary effect, there is also a permanent irreversible change in the aerodynamic performance due to the erosion of various engine components. This effect will be discussed in another report. The temporary decrease in the power output is of serious concern to aircrafts operating in the desert environment where apart from the airborne sand ingested while on take-off and landing, the occasional sand storm and the resulting relatively high concentration of sand can pose a serious threat to the operation of the aircraft. Many such incidences have been reported.

The phenomena of sand laden airflow through a turbomachine is treated as two phase flow. In most cases the solid particles mass concentration encountered is very low and subsequently the volume concentration is negligible. For example, even a mass of 2 gm/ft^3 is equivalent to about six percent mass concentration and a volume concentration of 2.8×10^{-3} percent only.

This low concentration enables one to neglect the particle-particle interaction and treat the individual particles. This approach was used by Tabakoff and Hussein [1] to compute

the particle trajectories and study the behavior of the individual particles through a given turbomachine. In addition, they also included the inelastic collision between the particle and the solid surfaces in these computations by means of experimental correlations for the so-called restitution ratios. Experimental data for such ratios on the impact of sand and ash particles for a variety of target metals are available [2, 3]. Tabakoff and Hussein's approaches have led to successful computational models to predict the particle trajectories through turbomachines. They also studied the particulate flow influence on turbomachinery performance by using a simple one dimensional model [4]. It was assumed that two stream tubes exist in the flow field around a given airfoil - one at the pressure side and the other at the suction side. The gas flow without particles was used to determine the nondimensional area of these stream tubes and one dimensional gas particle (two phase) flow equations were solved along these stream tubes to obtain the particulate flow pressure distribution along the airfoil.

The above method was successfully applied by Tabakoff et al. [5] to an axial flow turbine. However, the particles used were corn cups which are lighter than sand particles and tend to follow closer to the fluid streamlines, while even a sand particle of 30-40 micron size does not follow the fluid streamline. The major limitation of this method stems from the fact that the assumption of particles following the fluid streamline is not valid for sand particles.

In order to fully understand the flow phenomena under sand laden conditions, experiments were conducted on NACA-65 series airfoil profiles in a specially built 2-D cascade tunnel. In addition, a theoretical analysis of the two dimensional inviscid incompressible particulate flow through cascades was carried out, which gives a new insight into the various aspects associated with particulate flow field.

DEVELOPMENT OF FLUID-PARTICLE FLOW EQUATIONS

The governing equations for two dimensional gas particulate flow are derived under the following assumptions:

(1) The particles are spherical in nature.

(2) The volume concentration of the particles are negligible and hence there is no particle-particle interaction.

(3) The particle-fluid coupling is only due to viscous drag forces and the coupling is one way, i.e. there is no momentum transfer from particle to fluid. The energy dissipation of the particle while deceleration is due to viscous wake and this momentum does not contribute to an increase in fluid total pressure. This is due to the fact that the mean free path of the particle is very large as compared to the particle diameter (very low volume fraction, Soo, S.L., Ref. [6]).

(4) Though the fluid particle interaction is due to viscous forces, the viscous effects are neglected in the fluid momentum equation and the fluid is treated as inviscid.

(5) The flow is incompressible and there is no heat transfer between the fluid and the particles.

(6) The particles are treated in the Lagrangian system and the fluid in the Eulerian system.

Eulerian Formulation of the Fluid Phase

The continuity and momentum equations of the fluid phase in Cartesian coordinates may be written as follows:

$$\frac{\partial u_g}{\partial x} + \frac{\partial v_g}{\partial y} = 0 \tag{1}$$

$$u_g \frac{\partial u_g}{\partial x} + v_g \frac{\partial u_g}{\partial y} = - \frac{1}{\rho_g} \frac{\partial p}{\partial x} - \frac{F_x}{\rho_g} \tag{2}$$

$$u_g \frac{\partial v_g}{\partial x} + v_g \frac{\partial v_g}{\partial y} = - \frac{1}{\rho_g} \frac{\partial p}{\partial y} - \frac{F_y}{\rho_g} \tag{3}$$

where F_x and F_y are the interphase force term and represents the momentum transfer between the fluid and particles which will be treated later.

Equations (2) and (3) can be reduced together with equation (1) to give:

$$u_g \frac{\partial \omega}{\partial x} + v_g \frac{\partial \omega}{\partial y} = - \frac{1}{\rho_g} \frac{\partial F_x}{\partial y} + \frac{1}{\rho_g} \frac{\partial F_y}{\partial x} \tag{4}$$

where ω is the vorticity defined as

$$\frac{\partial u_g}{\partial y} - \frac{\partial v_g}{\partial x} = \omega \tag{5}$$

The following relations for the definition of a stream function can be written:

$$u_g = \frac{w}{b\,\rho_g}\frac{\partial \psi}{\partial y} \quad , \quad v_g = -\frac{w}{b\,\rho_g}\frac{\partial \psi}{\partial x} \tag{6}$$

where w is the mass flow through cascade, and b is the blade height of the cascade. Equation (6) satisfies the continuity equation (1) and equations (4) and (5) then reduce to the conventional stream function vorticity formulation.

$$\frac{\partial \psi}{\partial y}\frac{\partial \omega}{\partial x} + \frac{\partial \psi}{\partial x}\frac{\partial \omega}{\partial y} = -\frac{1}{\rho_g k}\frac{\partial F_x}{\partial y} + \frac{1}{\rho_g k}\frac{\partial F_y}{\partial x} \tag{7}$$

$$\frac{\partial^2 \psi}{\partial x^2} + \frac{\partial^2 \psi}{\partial y^2} = \frac{\omega}{k} \tag{8}$$

where

$$k = \frac{w}{b\,\rho_g} \quad .$$

Such formulation of equations (7) and (8) are easier to handle in a body fitted coordinate system. One may define a coordinate transformation such that

$$\eta = f_1(x,y) \quad , \quad \xi = f_2(x,y) \tag{9}$$

Then the above equations reduce to

$$\omega_\xi \psi_\eta - \omega_\eta \psi_\xi = \frac{1}{k\,\rho_g}\left[-x_\xi F_{x\eta} + x_\eta F_{x\xi} + y_\eta F_{y\xi} - y_\xi F_{y\eta}\right] \tag{10}$$

and

$$\left(\frac{\partial\left(\frac{\alpha}{J}\right)}{\partial\xi} - \frac{\partial\left(\frac{\beta}{J}\right)}{\partial\eta}\right)\frac{\partial\psi}{\partial\xi} + \left(\frac{\partial\left(\frac{\gamma}{J}\right)}{\partial\eta} - \frac{\partial\left(\frac{\beta}{J}\right)}{\partial\eta}\right)\frac{\partial\psi}{\partial\eta} + \frac{\alpha}{J}\frac{\partial^2\psi}{\partial\xi^2}$$

$$+ \frac{\gamma}{J}\frac{\partial^2\psi}{\partial\eta^2} - 2\frac{\beta}{J}\frac{\partial^2\psi}{\partial\xi\partial\eta} = \frac{J\omega}{k} \quad . \tag{11}$$

where

$$\alpha = x_\eta^2 + y_\eta^2 \quad , \qquad \beta = x_\xi x_\eta + y_\xi y_\eta \quad ,$$

$$J = x_\xi y_\eta - x_\eta y_\xi \quad , \qquad \gamma = x_\xi^2 + y_\xi^2 \tag{12}$$

There are many choices for the functions f_1 and f_2. Referring to Fig. 1, one can define that the lines of constant ξ and lines of constant x are the same, i.e. $\xi = x$. This will help to impose the periodicity boundary condition for the cascade flow, then

$$x_\eta = 0.0 \quad , \qquad x_\xi = 1.0 \quad ,$$

$$\alpha = y_\eta^2 \quad , \qquad \beta = y_\eta y_\xi \quad , \tag{13}$$

$$\gamma = 1 + y_\xi^2 \quad , \qquad J = y_\eta$$

and the vorticity transport equation (10) is modified as

$$\omega_\xi\psi_\eta - \omega_\eta\psi_\xi = \frac{1}{k\rho_g}\left[-F_{x_\eta} + y_\eta F_{y_\xi} - y_\xi F_{y_\eta}\right] \tag{14}$$

One can apply the transformation to the original momentum equations (2) and (3) and separate the two pressure terms, resulting in the following equations for pressure:

$$P_\xi = - \rho_g u_g u_{g_\xi} + \rho_g u_g \frac{y_\xi}{y_\eta} u_{g_\eta} - \frac{\rho_g v_g}{y_\eta} u_\eta + \frac{\rho_g u_g y_\xi^2}{y_\eta} v_{g_\eta}$$

$$- \rho_g u_g y_\xi v_{g_\xi} - \frac{\rho_g v_g y_\xi}{y_\xi} v_{g_\eta} - y_\xi F_y - F_x \qquad (15)$$

$$P_\eta = - \rho_g u_g y_\eta v_{g_\xi} + \rho_g u_g y_\xi v_{g_\eta} - \rho_g v_g v_{g_\eta} - y_\eta F_y \qquad (16)$$

From the solution of equations (11) and (14), one obtains the flow field. Equations (15) and (16) are then used to evaluate the pressure by integrating these equations for the given inlet conditions to the cascade. The boundary conditions, the method of solution and the choice of the function $\eta = f(x,y)$ are discussed in Appendix A.

Lagrangian Formulation of the Particle Phase

As mentioned earlier, it is assumed that only the fluid drag is the major force acting on the particles. The equation of motion of the single particle in Cartesian coordinates is given by:

$$m_p \frac{du_p}{dt} = D_x \qquad (17)$$

$$m_p \frac{dv_p}{dt} = D_y \qquad (18)$$

where D_x and D_y are the drag forces experienced by the particle, m_p is their mass, and u_p, v_p are particle velocities in x and

y directions. It is assumed that the particles are spherical and the drag forces are given by:

$$D_x = 3\pi\mu_g\, d_p\, f(Re)\,(u_g - u_p) \tag{19}$$

$$D_y = 3\pi\mu_g\, d_p\, f(Re)\,(v_g - v_p) \tag{20}$$

where

$$f(Re) = C_D \frac{Re}{24} \tag{21}$$

$$\begin{aligned} C_D &= \frac{24}{Re} && 0 < Re \leq 1.0 \\ C_D &= \frac{24}{Re}\left(1 + \frac{3}{16} Re\right) && 1.0 < Re \leq 4.0 \\ C_D &= 21.9416\, Re^{-0.718} + 0.3240 && 4 < Re \leq 2000 \\ C_D &= 0.4 && 2000 < Re \leq 3 \times 10^4 \end{aligned} \tag{22}$$

The Reynolds number in equations (19-22) is given by:

$$Re = \frac{d_p \rho_g}{\mu_g} \cdot \sqrt{(u_g - u_p)^2 + (v_g - v_p)^2} \tag{23}$$

Particle Dynamics

The equations of motion for the particles are solved by time marching technique [7]. At each time step knowing the particle location, the flow properties are computed by interpolation. Then the particles drag forces and accelerations are calculated. If the particle impacts on the solid boundary, then the exact impact point is located by Newton-Raphson

iteration technique. At this point the experimental correlation data for the restitution ratios is applied.

The magnitude and direction of the particle rebounding velocity after collision with a solid surface must be known in order that the solution of the particle equations of motion be continued beyond the point of collision. An experimental study was conducted to investigate the particle impact-rebound characteristics. The following correlations were derived for 165 micron quartz particles impacting aluminum 6064 metal surface.

Normal restitution ratio

$$\frac{V_{n_2}}{V_{n_1}} = 0.993 - 1.76\ \beta_1 + 1.56\ \beta_1^2 - 0.49\ \beta_1^3 \qquad (24)$$

Tangential restitution ratio

$$\frac{V_{t_2}}{V_{t_1}} = 0.998 - 1.66\ \beta_1 + 2.11\ \beta_1^2 - 0.67\ \beta_1^3 \qquad (25)$$

where V_{n_1} and V_{n_2} are the impinging and rebounding particle velocity components normal to the impacting surface and V_{t_1} and V_{t_2} are the tangential components parallel to the impacting surface. The angle between the incoming particle and the solid surface is denoted by β_1.

The solution of equations (24) and (25) at the point of impact gives the rebounding particle velocity components. The

solution of the particle equations of motion is continued from the impact point until the particles exit the downstream boundary of the cascade.

Computation of the Interphase Force Terms

The computation of the force terms at each grid point where the fluid solution is to be found is based on the method employed by Crowe [8]. The average interphase force terms can be evaluated at any grid point i,j by considering a cell ABCD surrounding the grid point i,j as shown in Fig. 2.

Since the number of particles entering the cascade can be very large, it is assumed that each trajectory line, I, computed through the cascade is associated with a particular mass fraction of X^I. If the total particles mass entering the cascade is $\dot{M}_p$, then the total number of particles represented by any trajectory line is given by:

$$\dot{n}_p^I = X^I \dot{M}_p / m_p \tag{26}$$

where m_p is the mass of the single particle.

The number density of the particles in cell i,j due to the trajectory I is given by:

$$n_{p_{i,j}}^I = \dot{n}_p^I \Delta\tau / V_{cell_{i,j}} \tag{27}$$

where v_{cell} = cell volume, and $\Delta\tau$ is the residence time of the particles inside the cell ABCD associated with the trajectory line I.

The interphase force terms are

$$f^I_{x_{i,j}} = n^I_{p_{i,j}} \bar{\dot{u}}^I_{p_{i,j}} \tag{28}$$

$$f^I_{y_{i,j}} = n^I_{p_{i,j}} \bar{\dot{v}}^I_{i,j} \tag{29}$$

where $\bar{\dot{u}}^I_{p_{i,j}}$ and $\bar{\dot{v}}^I_{p_{i,j}}$ are the average particle accelerations associated with trajectory I through the cell i,j.

The total force terms $F_{x_{i,j}}$ and $F_{y_{i,j}}$ are the sum of the forces associated with all trajectories at cell i,j, i.e.,

$$F_{x_{i,j}} = \sum_{I=1}^{N} f^I_{x_{i,j}} \tag{30}$$

and

$$F_{y_{i,j}} = \sum_{I=1}^{N} f^I_{y_{i,j}} \tag{31}$$

These forces are then used in the computations of the flow field with particle presence.

EXPERIMENTAL FACILITY

The design of the experimental set-up to study particulate flow through cascades is complicated. The most important constraints are to insure a good distribution of the particle concentration and particle velocity on the entire test section. Such distribution of particle concentration is difficult to achieve in a horizontal tunnel. In addition the constant area duct of the tunnel to the entrance of the test section needs to be of specified length to accelerate the particles to a reasonably high velocity. However such a long constant area duct is associated with a rapid boundary layer growth and hence is not well suited for the purpose of cascade studies. Any attempt to provide boundary layer control with the use of porous tunnel walls is rendered futile, since the particles can block off the porous walls as well as erode the surface away. The problem was overcome by providing a sudden contraction just before the test section to remove any very low velocity fluid near the entrance to the test section. This sudden contraction proved to be of great help in providing a reasonably uniform flow at the cascade test section over about 80 percent of the test section area.

A schematic configuration of the tunnel is shown in Fig. 3. It consists of the following components: particle feeder (A), main air supply pipe (B), settling chamber and particle injector (C), accelerating tunnel (D), test section (E), and exhaust tank (F). The equipment functions as follows: a measured amount

of abrasive grit of a given constituency is placed into the particle feeder (A). The particles are fed into a secondary air source and blown up to the particle injector in the settling chamber (C), where it mixes with the main air supply (B). The particles are accelerated by the high velocity air in the constant area duct (D), before impacting the cascades in the test section (E). Past the test section the particulate flow is exhausted through exhaust collector (F).

Since the particles are accelerated in the constant area duct by the aerodynamic drag forces, their velocity before impacting the cascade would depend upon the air velocity, the particle size and the length of the acceleration section (D). Figure 4 gives an illustration of the dynamics of relatively large 165 micron particles with air flow velocity of 130 m/s. From this figure it can be seen that the particles final velocity is an exponential function of the tunnel length. Based on these findings, a tunnel length of 3 meters was used in obtaining the experimental data. The test section (E) of rectangular cross section 37.5 mm x 135 mm, was slightly smaller in cross section than the accelerating duct (D) and is fitted with transparent walls. High speed photographic technique was used to study the sand particles in this section. In this manner the velocity of the approaching sand particles was obtained and compared to the theoretical predictions. In addition the particle distribution was studied by sampling the flow in different locations.

Instrumentation

The primary and secondary air mass flow rates were measured using standard ASME orifice flow meters. The blade surface pressure distribution, the total pressure in the settling chamber, and the test section wall static pressures were measured using a scanivalve-pressure transducer-digital recorder system.

RESULTS AND DISCUSSIONS

Experimental Results

For the purpose of comparison experiments were conducted on three different cascades according to NACA 65-(10)10 airfoil specifications [9]. The airfoils were made of 6064-T6 Aluminum and produced by extrusion process. The chord of these airfoils were 50.8 mm. These airfoils were tested at a space chord ratio of 0.5. The low space chord ratio was chosen to ensure a minimum of five blade passages in the tunnel cascade. All the measurements were taken in the cascade center passage. The locations of the surface pressure taps are as shown in Fig. 5 and their axial positions are as given in Table I.

The experiments were conducted on three different cascades. One was an accelerating cascade and the other two were diffusing cascades. The particles used were quartz sand of 165μ mean diameter. The details of the cascade inlet and exit angles and the stages and incidences are as shown in Table II. However it was observed that the stagger setting of the cascade II was wrong by 3° and the air inlet angle was wrong by 4°. The

air inlet angle changed, since the guides used to locate the cascade were eroded by the sand resulting in improper positioning of the cascades with reference to the air flow direction. This problem was later corrected in the testing of the third cascade.

All the experiments were conducted at an inlet air velocity of 130 m/sec, which corresponded to a particle velocity of about 100 m/sec. Figure 6 shows the surface pressure measurements in absolute quantities as obtained in a particular test.

Inspection of this figure shows that the overall static pressure level increases in the entire cascade with the injection of sand in the tunnel. This is from the increased resistance to the flow due to the presence of the particle in the piping system. In addition, attempts made to measure the total pressure with the particles flowing proved to be futile, since the particles clogged up the probes. The only pressure measurements that were carried out were the blade surface pressures in the cascade passage, the inlet and the exit wall static pressures. However it was noted that the inlet and exit wall static pressures increased nearly by the same amount with the presence of the particles. Since the air mass flow through the tunnel did not change, and the change in the air density at the test section was negligible, the inlet total pressure was computed as the sum of the inlet dynamic head and the inlet wall static pressure.

For a better understanding of the results, they are presented in the form of nondimensional pressure coefficient, S, which is defined as:

$$S = \frac{P_{t_i} - P_s}{P_{t_i} - P_i} = \frac{P_{t_i} - P_s}{q_i}$$

where P_{t_i} is the inlet total pressure,

P_s is the surface static pressure,

P_i is the inlet static pressure, and

q_i is the inlet dynamic head.

Figures 7 through 9 show the observed results. From the inspection of these figures, it can be seen that the change due to particulate flow, in the surface pressure distribution measured does not follow a specific pattern. In the case of the accelerating cascade, Fig. 7, there is a uniform change on the blade suction side and there is a significant change in the rear half of the blade pressure side. These changes are in the same direction and the decrease in the pressure coefficient indicates a higher surface static pressure. In the case of the diffusing cascade, it can be noted from Figs. 8 and 9 that the overall tendancy is a decrease in the pressure coefficients on both surfaces. Since, for most part of the blade surfaces, the pressure coefficient with particulate flow decreases, one can conclude that there is an increase in the surface static pressures.

Theoretical Results

Using the analytical approach described earlier, the results for the same three cascades are presented in Figures 10 through 23. The trajectories through accelerating cascade for three different size particles 5, 10 and 165 microns in diameter are shown in

Figures 10, 11 and 12 respectively. Figures 13, 14 and 15 show the trajectories of the 5, 10 and 165 micron particles through the diffusing cascade III. From these figures it can be seen that the large particles are least influenced by the air, while the small particles are highly influenced. However, the particles are more influenced in the case of the accelerating cascade than in the case of the diffusing cascade. In addition, it can be observed that there is a region of no particles on the rear half of the blade suction surface. It can also be concluded from these figures that the particle local concentration can be much higher than the mean concentration, particularly near the blade pressure surface.

Figures 16 and 17 show the streamline patterns with and without particles, for two cascades. In both cases, the concentration of particles is 10% and the particle diameter is 165 microns. The streamlines with particulate flow bend away from the blade pressure surface towards the suction surface. However, these changes can be clearly seen only close and beyond the trailing edges of the cascades. The maximum change was only of the order of few percent. The movement of the streamlines away from the blade pressure surface results in a decrease in velocities on the pressure surface and the movement of the streamlines closer to the suction surface results in an increase in the velocities on the suction surface.

Figures 18, 19, 20 and 21 show the effect of the particles on the cascade pressure distribution. The change in the blade surface pressure coefficients for the three cascades considered,

at identical particle and air velocities for $\alpha = 0.10$ and $d_p = 165$ microns, are shown in Figures 18, 19 and 20. The effect of the particles show decrease on the blade surface static pressures, especially on the blade suction surface. The pressure distribution on the blade pressure surface is more sensitive to the particle presence and does not follow an exact pattern in the case of these large particles. Figure 21 shows the effect of small partices, $d_p = 10$ microns, on one of the diffusing cascades. It can be seen from this figure that for very small particles, the pressure coefficient increases on both surfaces indicating a decrease in the surface static pressure on both surfaces. A simple explanation for this could be that there are two different phenomena happening inside the blade passages. First, the increased concentration of the particles near the blade pressure surface, results in a considerable decrease in the total pressure and velocities of the fluid near the blade pressure surface, which are accompanied by an increase in the fluid velocities on the blade suction surface. However, the fluid velocities are altered in such a way that the static pressure variation in the flow field satisfies the velocity distribution in the flow field. For this reason, the theoretical method predicts an overall decrease in the static pressure in the flow field. A comparison of the theoretical and experimental results indicates that there is small disagreement. The experimental results indicate small increase in the surface static pressures for the most part of the blade profile, while the theoretical results predict a small decrease in the surface static pressures.

There are many deficiencies both in the theoretical model and in the experimental techniques. The theoretical model, assumes incompressible flow, but the real flow is compressible. In addition, the theoretical model, assumes sharp leading and trailing edges. In the case of the experimental technique, the inlet total pressure could not be measured exactly and the inlet static pressure increases on introducing the particles. From the particle trajectories through the cascade one can observe an increased particles concentration near the blade pressure surfaces and it is possible that the local concentration can be suficiently high so that there is some contribution to the surface pressure changes. Furthermore, there is erosion taking place continuously as the testing progresses. In order to reduce any contribution from this aspect, the concentration has to be very low. However, at very low concentrations, the change in the pressure distributions can be so small, that it can not be measured. In addition, the measured surface pressure distributions are time averaged values using the scanivalve system. There could be considerable interaction between the pressure measurement system and the continuously changing surface static pressures. The tests on cascade III were carried out using multitube manometer instead of the scanivalve system. During these tests it was observed that the surface static pressure was continuously fluctuating during the entire testing period on introduction of the particles. All of the above mentioned problems could be the reason why the small difference exists between the experimental and theoretical results.

The mean exit total pressure of the cascade is always less than the mean inlet total pressure under particulate flow conditions. The theoretical analysis was carried out for various particle sizes from 10 to 250 microns diameter and particle concentrations of 5 to 20 percent.

Based on the mean exit total pressure, a loss coefficient, ζ, due to the presence of particles can be defined as follows:

$$\zeta_{particle} = \frac{\bar{P}_{t_i} - \bar{P}_{t_e}}{\bar{q}_i}$$

where $\bar{P}_{t_i}$ = mean inlet total pressure,
$\bar{P}_{t_e}$ = mean exit total pressure,
$\bar{q}_i$ = mean inlet dynamic head.

Figure 22 shows the effect of particle diameter on the total pressure loss for two of the cascades considered for the same particle concentration. The total pressure loss is much higher for the case of the accelerating cascade and the total pressure loss decreases rapidly as the particle size increases to a very low level. Under identical conditions, the fluid drag is proportional to the total surface area of the particles. For the same particle concentration, the total surface area is proportional to $1/d_p$. For this reason, the small particles give rise to a large decrease in total pressure. In the case of the decelerating cascade, the difference in velocities

between the rebounding particles and the fluid is not as high as in the case of the accelerating cascade. This leads to the loss coefficient in decelerating cascades being normally lower than that in accelerating cascades. The effect of concentration on the loss coefficient is shown in Fig. 23 for the two cascades considered. It can be observed that the loss coefficient increases linearly with the particle concentration. In order to enable comparison under identical conditions, the particle velocity to air velocity ratio at the inlet of the cascade was the same in all the cases. In a real situation, the velocities of the smaller particles will be close to the air velocities. Consequently, the total pressure loss coefficients may not be as high as indicated in Fig. 22 for the small particles.

CONCLUSIONS

The experimental investigation on particulate flow through air foils in cascade shows a small decrease in blade surface pressure coefficients with the presence of particles. The theoretical analysis indicates that the streamlines bend towards the suction surface with the introduction of the particles. Though the theoretical analysis also shows only a small change in the pressure coefficients with the introduction of the particles, the pressure coefficients were found to increase with the presence of particles. The reason for this difference could be mainly from the interaction between the pressure measurement system and the effect of particles on the flow conditions in the cascade tunnel like increased turbulance level and back pressure. The theoretical analysis also predicts the total pressure loss

associated with the particulate flow. This loss is found to be directly proportioned to the particle concentration. The total pressure loss is considerably higher for smaller particles than bigger particles under identical inlet conditions to the cascade. In a real situation the ratio of particle velocity to the air velocity will be higher for the smaller particles as compared to the big particles, and the total pressure loss may be slightly different than that used for comparison. However, this loss in total pressure can significantly alter the pressure ratios in a multistage machine, leading to a considerable decrease in the performance.

REFERENCES

1. Tabakoff, W. and Hussein, M.F., "Trajectories of Particles Suspended in Fluid Flow Through Cascades," Journal of Aircraft, Vol. 8, No.1, January 1971.

2. Grant, G. and Tabakoff, W., "Erosion Prediction in Turbomachinery Due to Environmental Solid Particles," AIAA Paper No. 74-16, AIAA 12th Aerospace Sciences Meeting, Washington, D.C., January 30-February 1, 1974.

3. Wakeman, T. and Tabakoff, W., "Measured Particle Rebound Characteristics Useful for Erosion Prediction," ASME Paper No. 82-GT-10.

4. Tabakoff, W. and Hussein, M.F., "Effect of Suspended Solid Particles on the Properties in Cascade Flow," AIAA Journal, Vol. 8, August 1971, pp. 1514-1519.

5. Tabakoff, W., Hosny, W. and Hamed, A., "Effect of Solid Particles on Turbine Performance," Journal of Engineering for Power, January 1976.

6. Soo, S.L., Fluid Dynamics of Multi-Phase System, Blaisdell Publishing Co.

7. Hussein, M.F. and Tabakoff, W., "Dynamic Behavior of Solid Particles Suspended by Polluted Flow in a Turbine Stage," Journal of Aircraft, Vol. 10, No. 7, July 1973.

8. Crowe, C.T. and Stock, D.E., "A Computer Solution for Two Dimensional Fluid Particle Flows," International Journal for Numerical Methods in Engineering, Vol. 10, 1976, pp. 185-196.

9. Emery, J.C., Herring, L.J., Erwin, J.R. and Felix, A.R., "Systematic Two-Dimensional Cascade Tests of NACA-65 Series Compressor Blades at Low Speeds," NACA Report 1368.

10. Vavra, M.H., Aerothermodynamics and Flow in Turbomachines, John Wiley and Sons, Inc., New York, London, 1960.

11. Roache, P.J., Computational Fluid Dynamics, Hermosa Publishers, Albuquerque, New Mexico.

12. Fox, L., Numerical Solution of Ordinary and Partial Differential Equations, Addison Wesley Publishing Co., Inc., Reading, Massachusetts, Palo Alto, London, 1962.

NOMENCLATURE

b	blade height in cascade, (m)
C_D	coefficient of drag
Ch	chord, (m)
C_{ax}	axial chord, (m)
d	diameter, (m)
D	drag force, (N)
F	interphase force, (N/m^3)
(i,j)	grid point indices
I	index of the trajectory
J	transformation parameter
k	constant defined as $W/b\rho_g$
$\dot{m}$	mass flow rate of particles along a trajectory (kg/sec)
m	mass
p	pressure, (N/m^2)
q	dynamic head, $\frac{1}{2}\rho V^2$, (N/m^2)
Re	Reynolds number
S	pressure coefficient
Δt	residence time, (sec)
u	velocity in the x direction, (m/sec)
$\bar{u}_p$	average acceleration of the particle in the x direction, (m/sec^2)
v	volume, (m^3)
$\bar{v}_p$	average acceleration of the particle in the y direction, (m/sec^2)
w	mass flow rate of gas through one cascade
(x,y)	Cartesian coordinates passage, (kg/sec)

α	transformation parameter or particle mass concentration
β	transformation parameter or angle
γ	transformation parameter
ζ	total pressure loss coefficient
μ	viscosity, (N sec/m^2)
(ξ,η)	transformed coordinates
ψ	stream function
ω	vorticity, (1/sec)

Subscripts

e	exit
g	gas
i	inlet
p	particle
t	total
(x,y)	x and y components
ξ,η	partial derivatives with reference to ξ, η

TABLE I

LOCATION OF SURFACE PRESSURE PROBES

Suction	Pressure	x/C_{ax}
S_1	P_1	0.040
S_2	P_2	0.125
S_3	P_3	0.250
S_4	P_4	0.350
S_5	P_5	0.475
S_6	P_6	0.625
S_7	P_7	0.725
S_8	P_8	0.825
S_9	P_9	0.890

TABLE II

DETAILS OF CASCADES USED IN TESTING PROGRAM

Parameter	Cascade I	Cascade II	Cascade III
Air Inlet Angle, β_1	0.0	35°	45°
Stagger	-20°	+15°	+25°
Camber θ	35°	35°	35°
Incidence	-3.00	-3.00	-3.00
Aspect Ratio	0.75	0.75	0.75
Pitch-Chord Ratio	0.5	0.5	0.5
No. of Blades	6	7	9

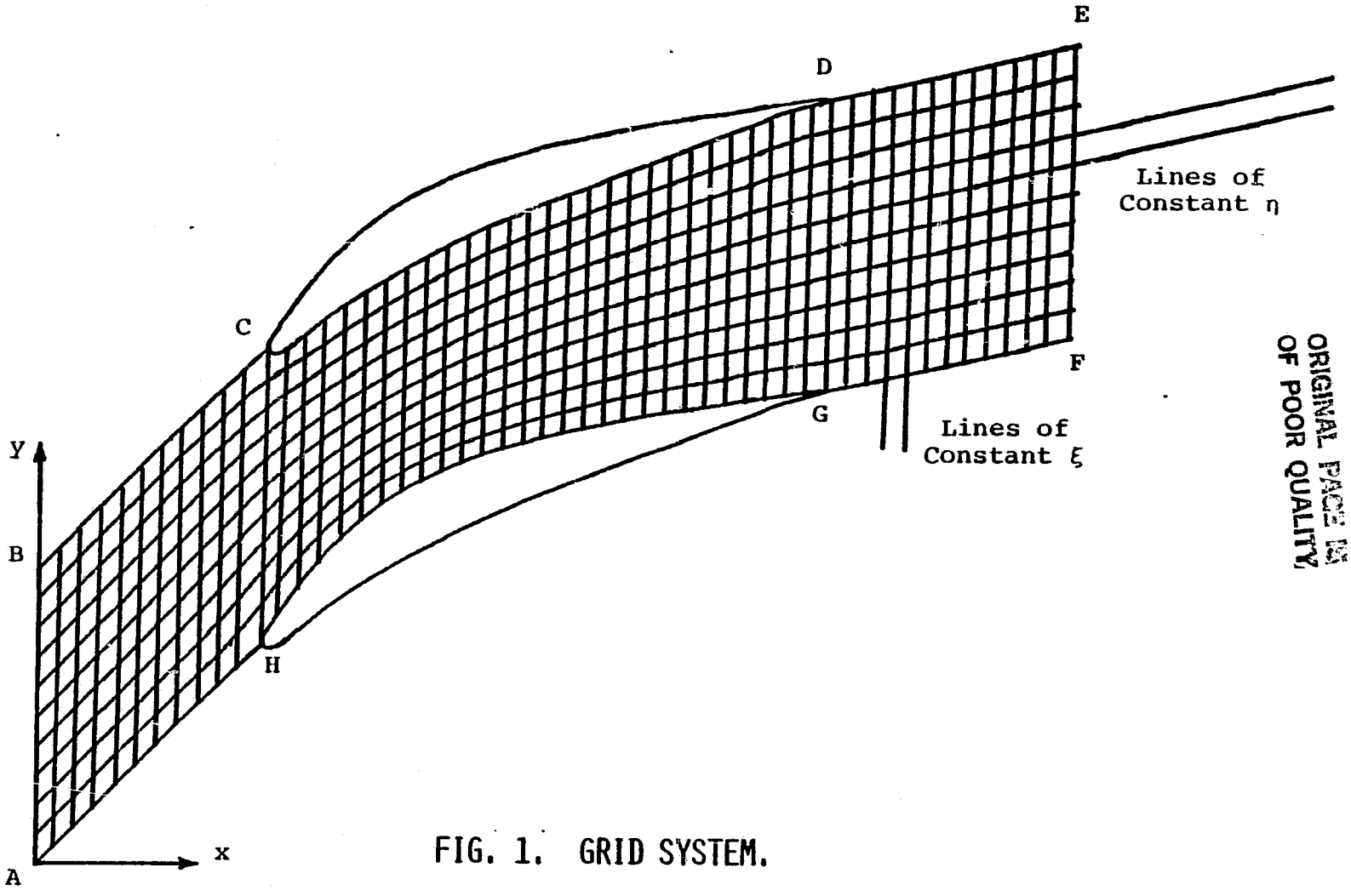

FIG. 1. GRID SYSTEM.

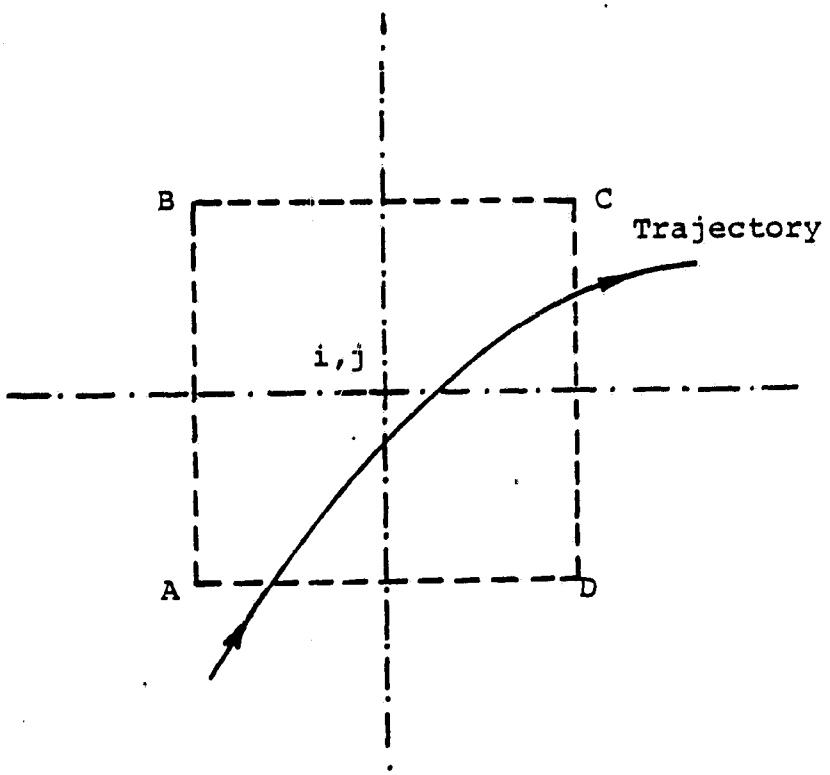

FIG. 2. CONTROL VOLUME FOR COMPUTING FORCE TERMS

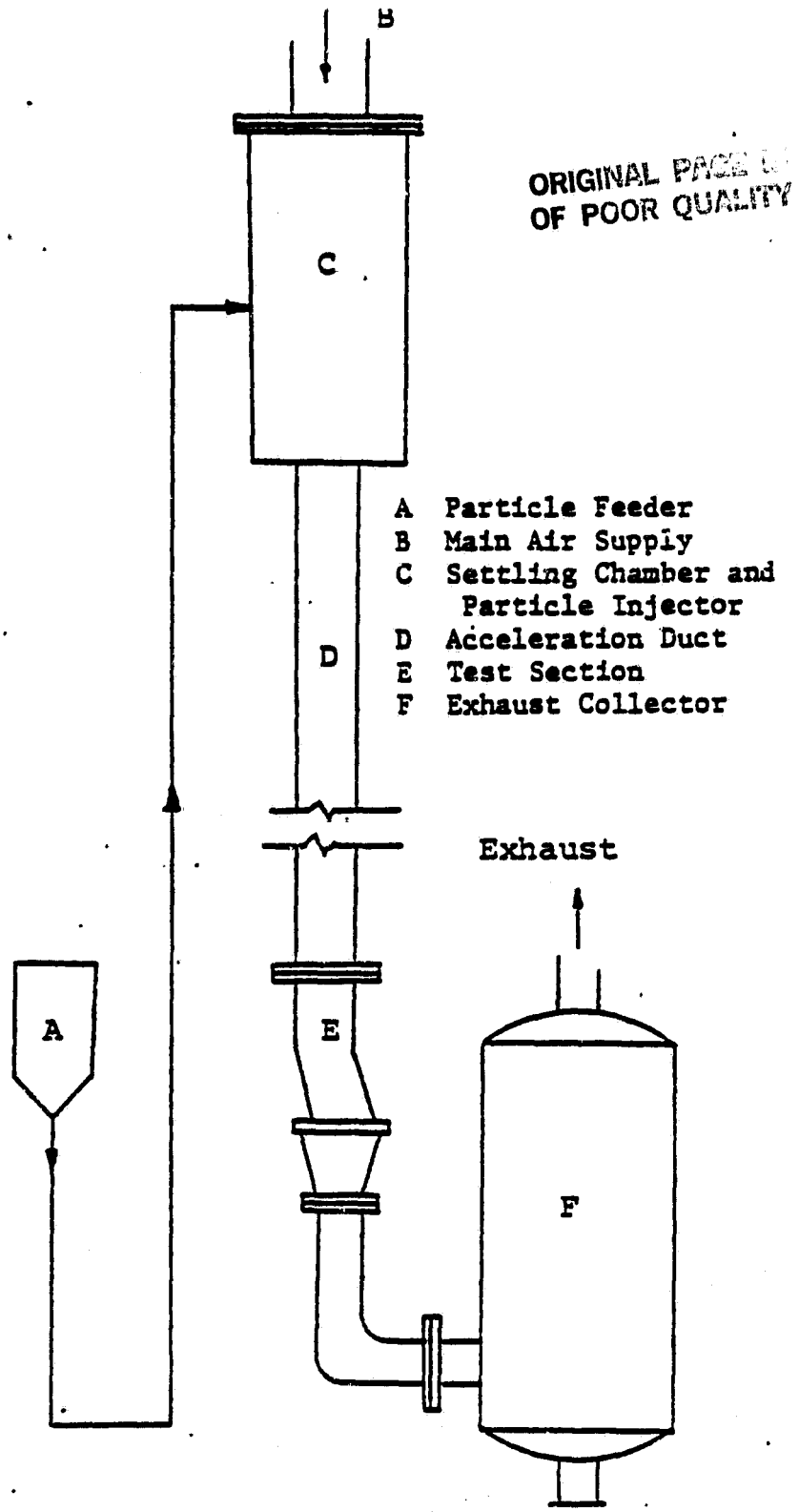

FIG. 3. SCHEMATIC OF CASCADE EROSION TUNNEL.

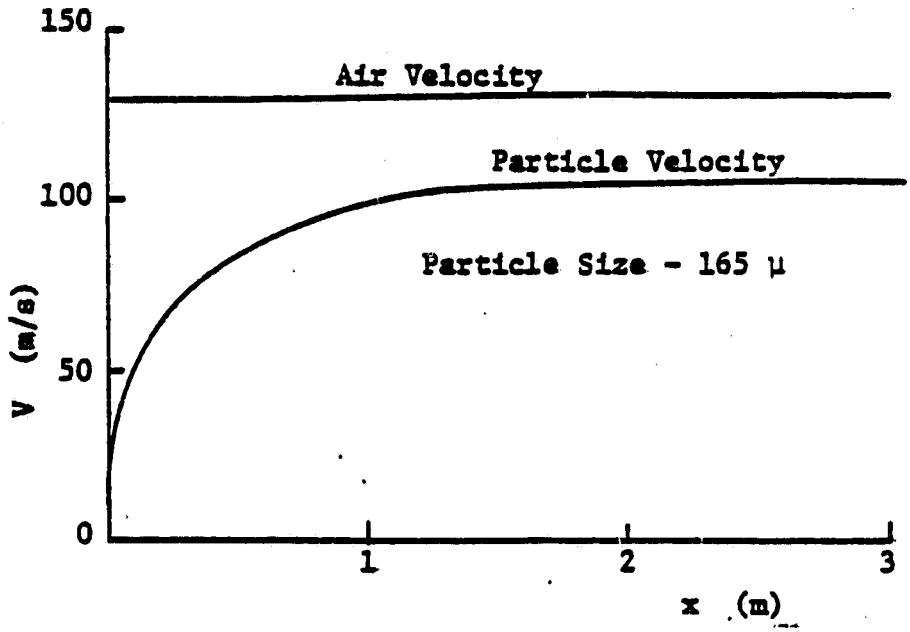

FIG. 4. PARTICLE VELOCITY ALONG THE TUNNEL.

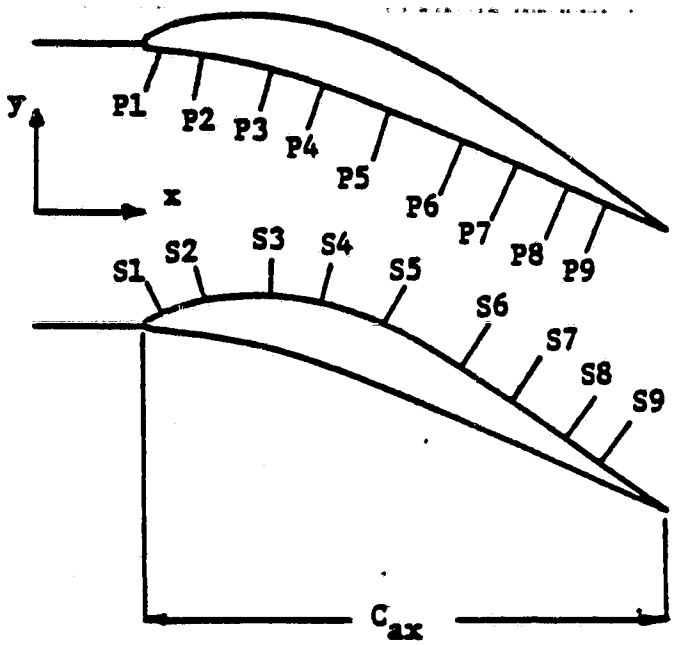

FIG. 5. SCHEMATIC OF PRESSURE TAP LOCATIONS.

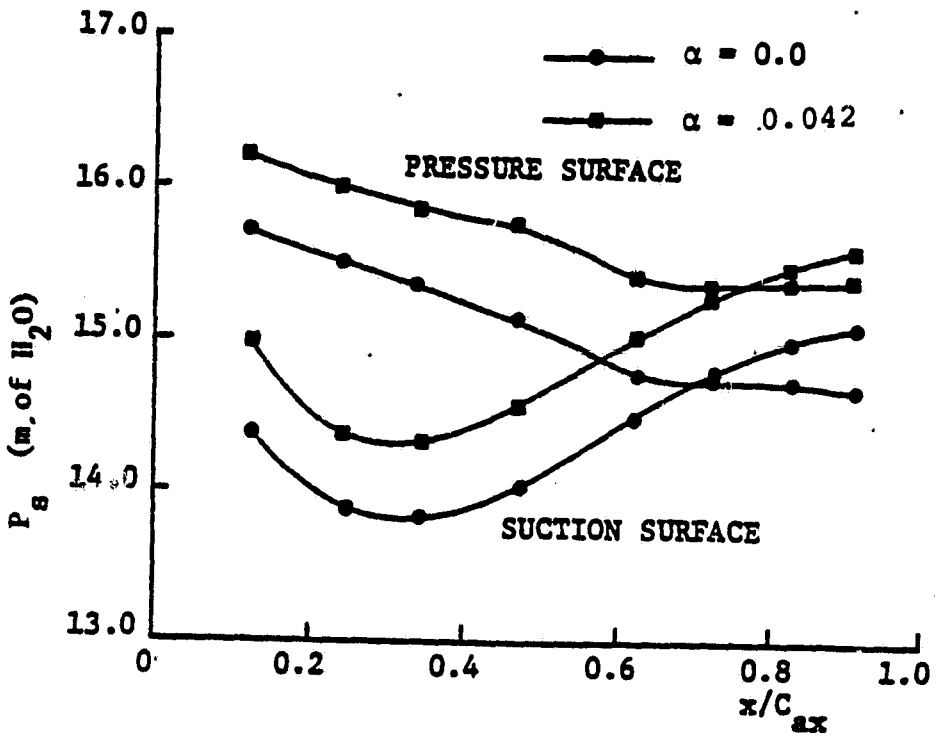

FIG. 6. MEASURED PRESSURE DISTRIBUTION OF CASCADE I.

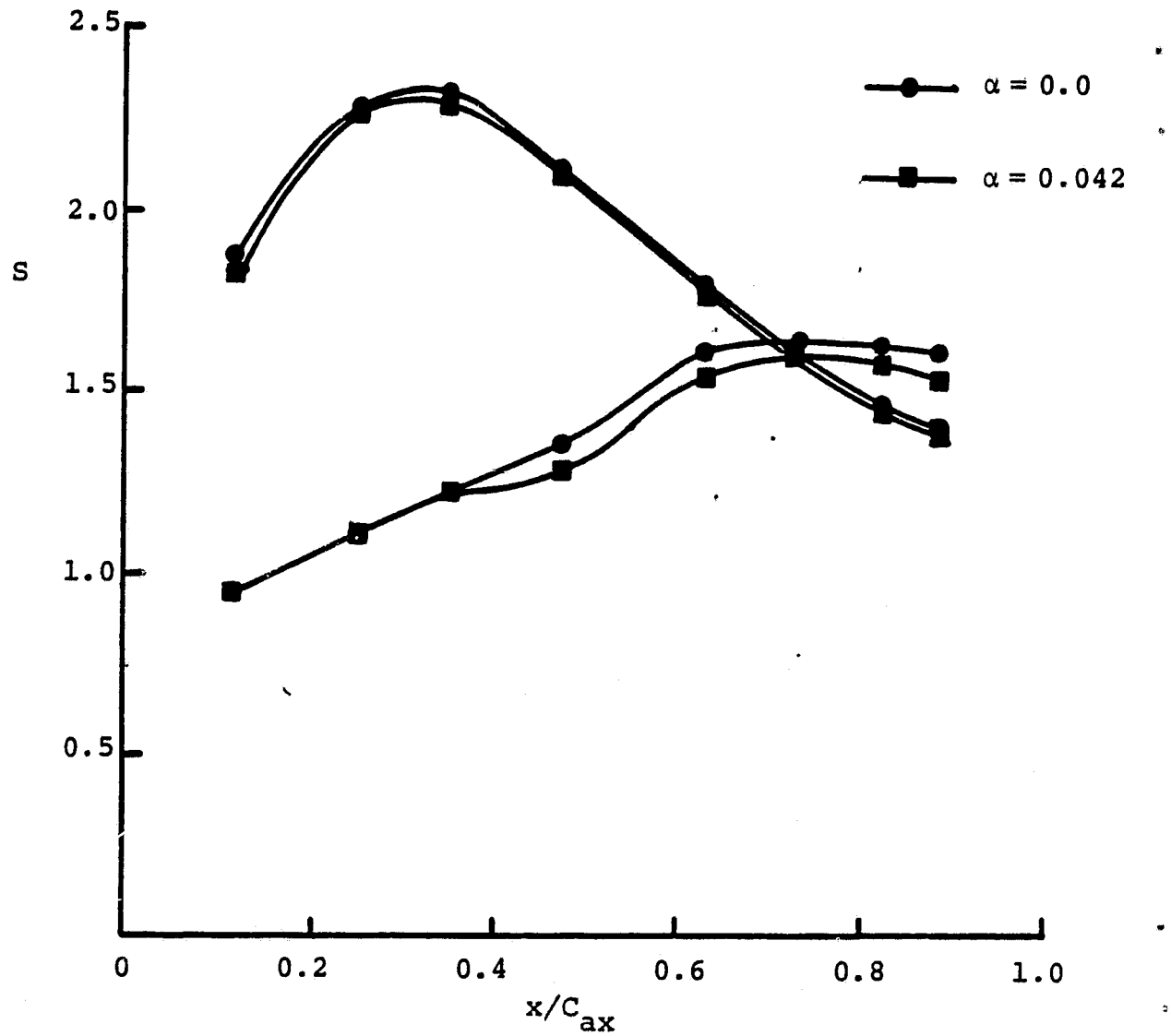

FIG. 7. MEASURED PRESSURE DISTRIBUTION OF CASCADE I FOR $\alpha = 0.0$ AND $\alpha = 0.042$.

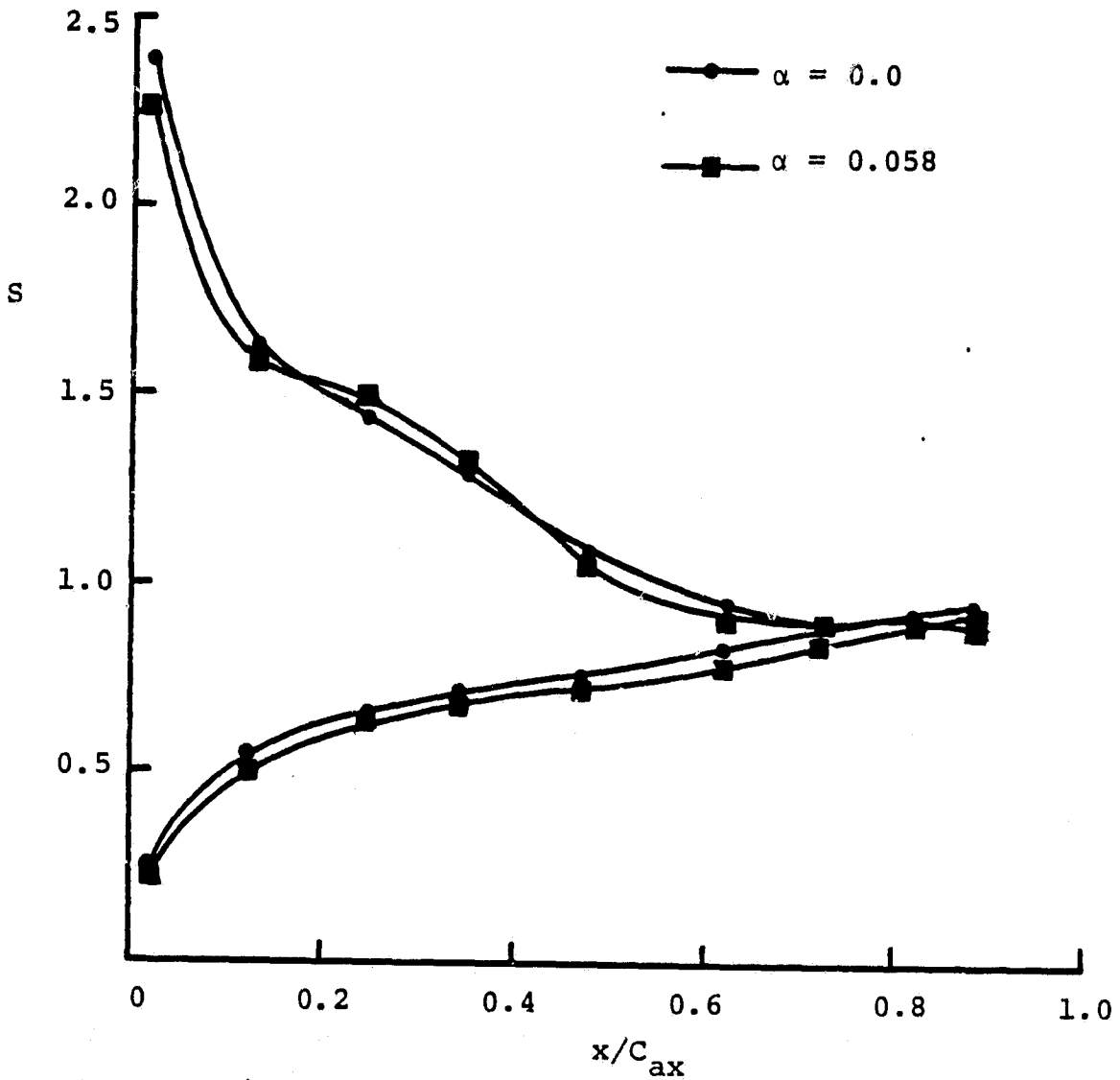

FIG. 8. MEASURED PRESSURE DISTRIBUTION OF CASCADE II FOR $\alpha = 0.0$ AND $\alpha = 0.058$.

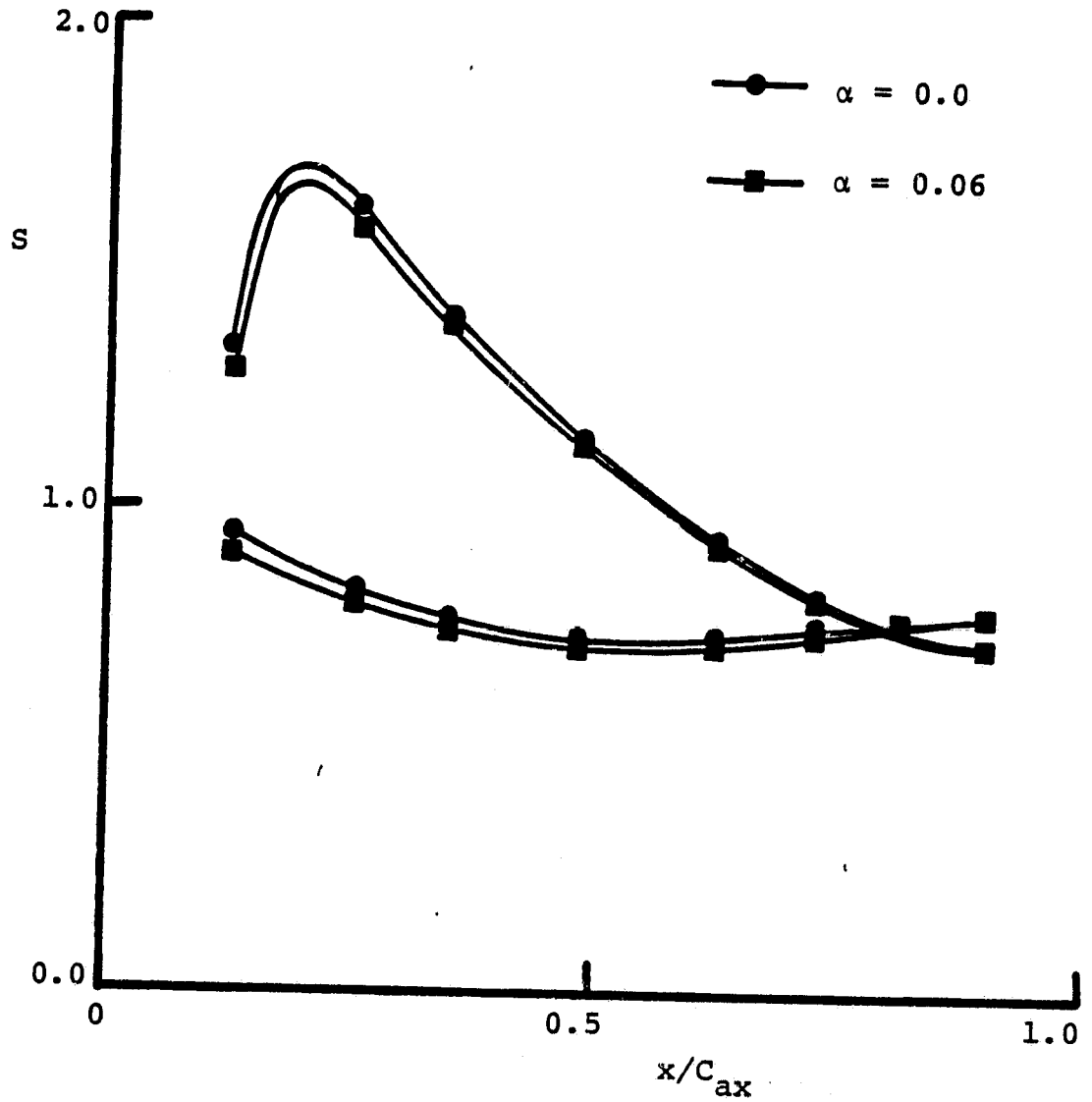

FIG. 9. MEASURED PRESSURE DISTRIBUTION OF CASCADE III FOR $\alpha = 0.0$ AND $\alpha = 0.06$.

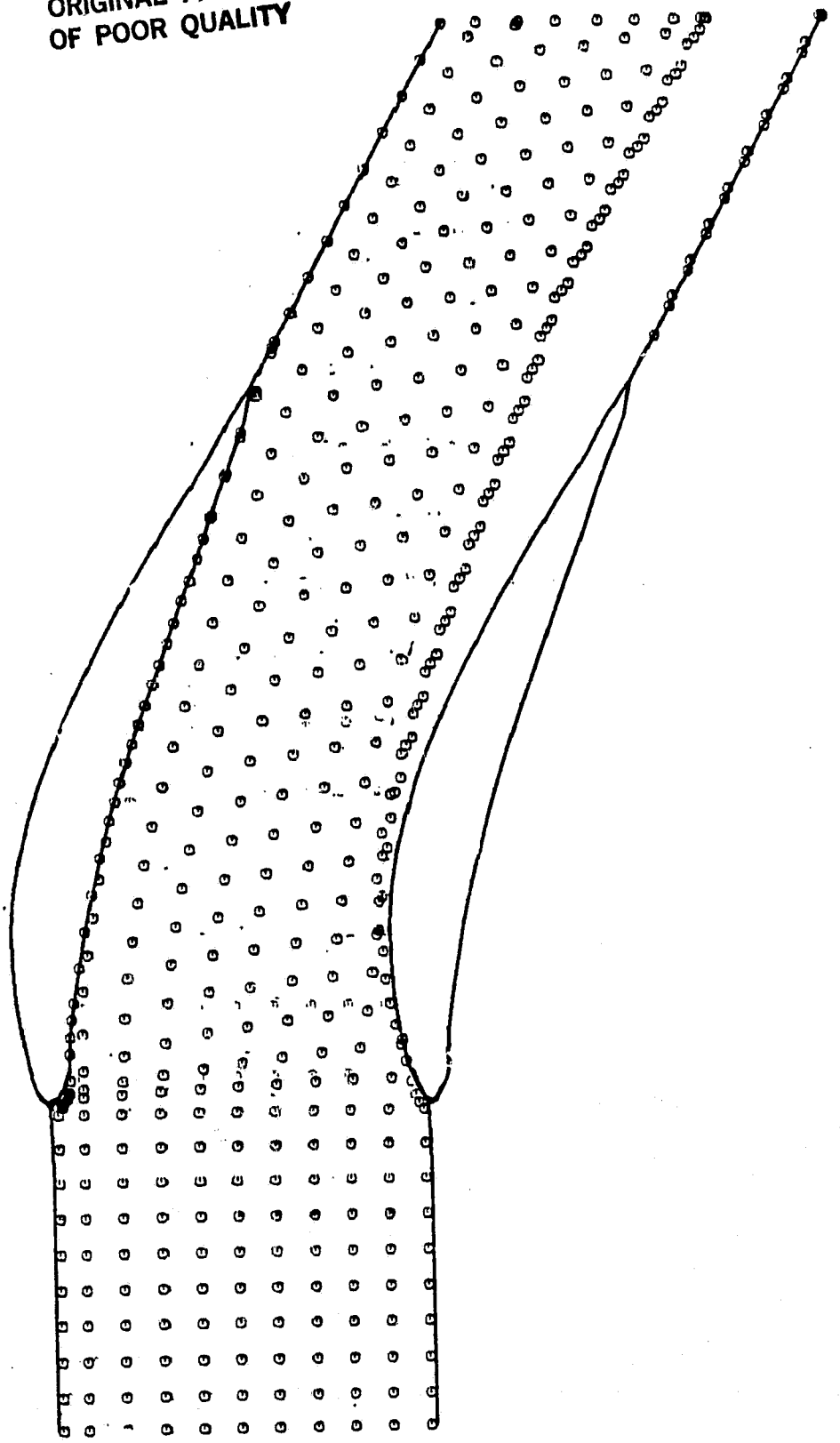

FIG. 10. PARTICLE TRAJECTORIES THROUGH CASCADE I,
d_p = 5 MICRONS.

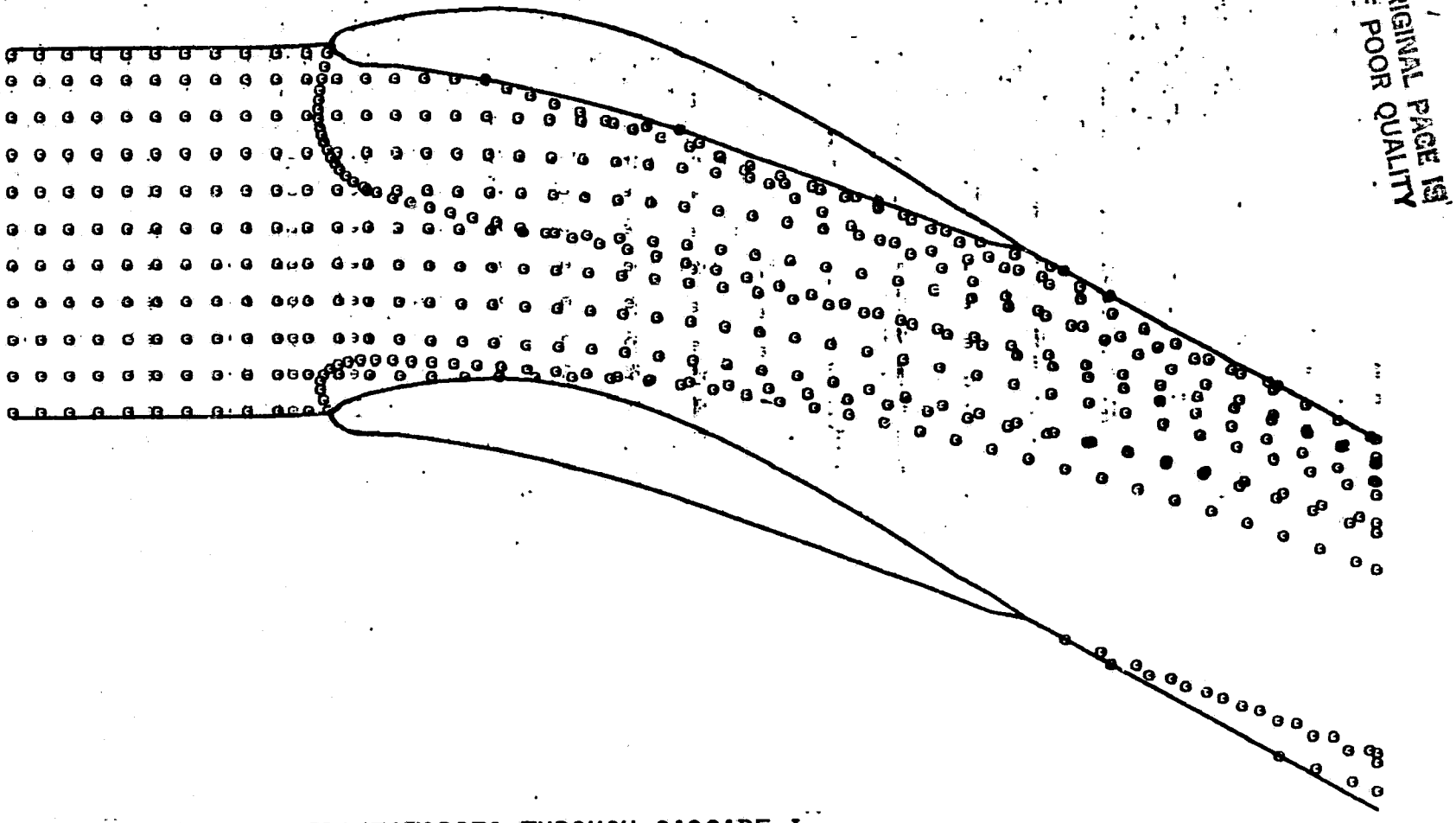

FIG. 11. PARTICLE TRAJECTORIES THROUGH CASCADE I,
d_p = 10 MICRONS.

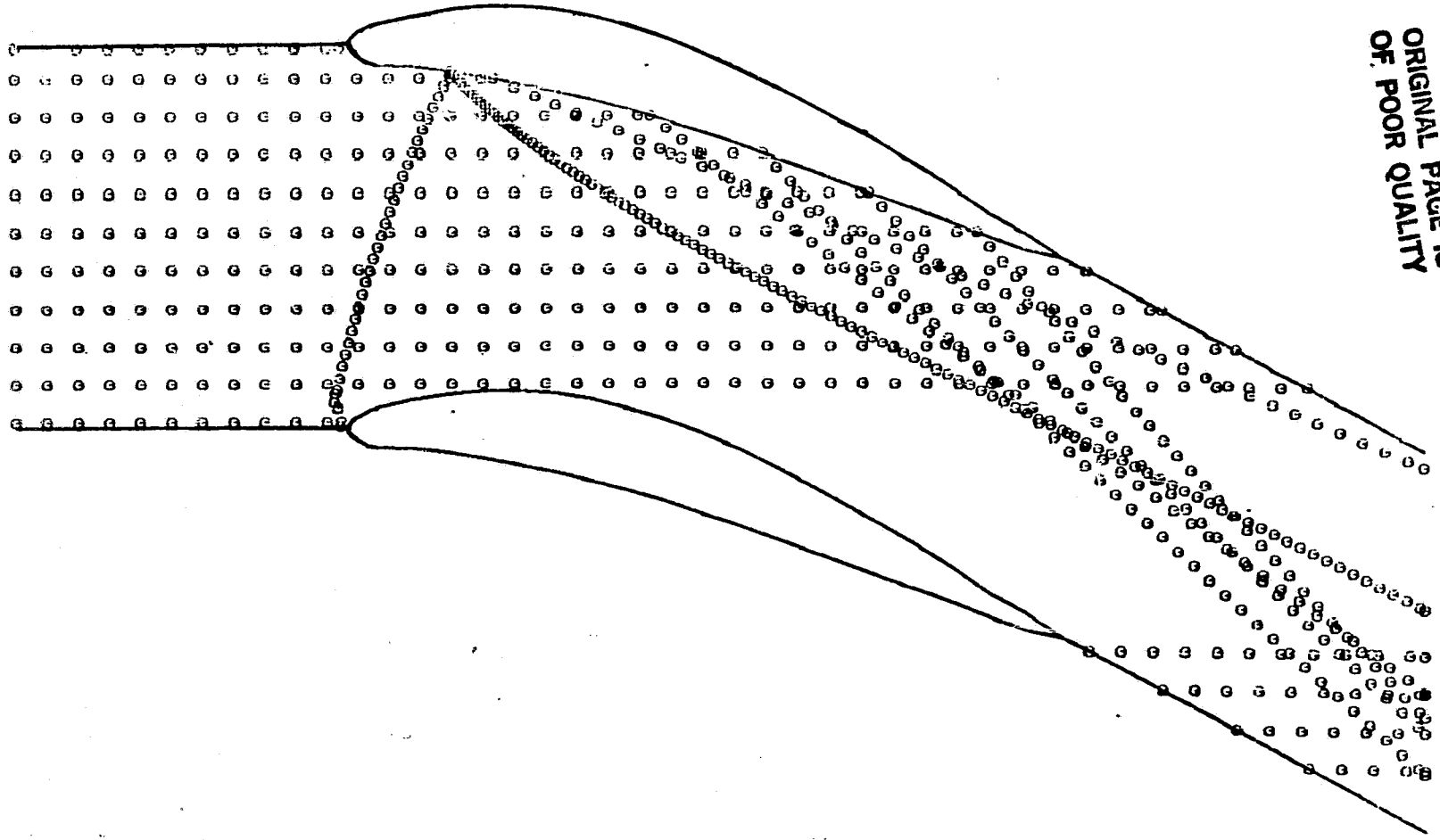

FIG. 12. PARTICLE TRAJECTORIES THROUGH CASCADE I,
d_p = 165 MICRONS.

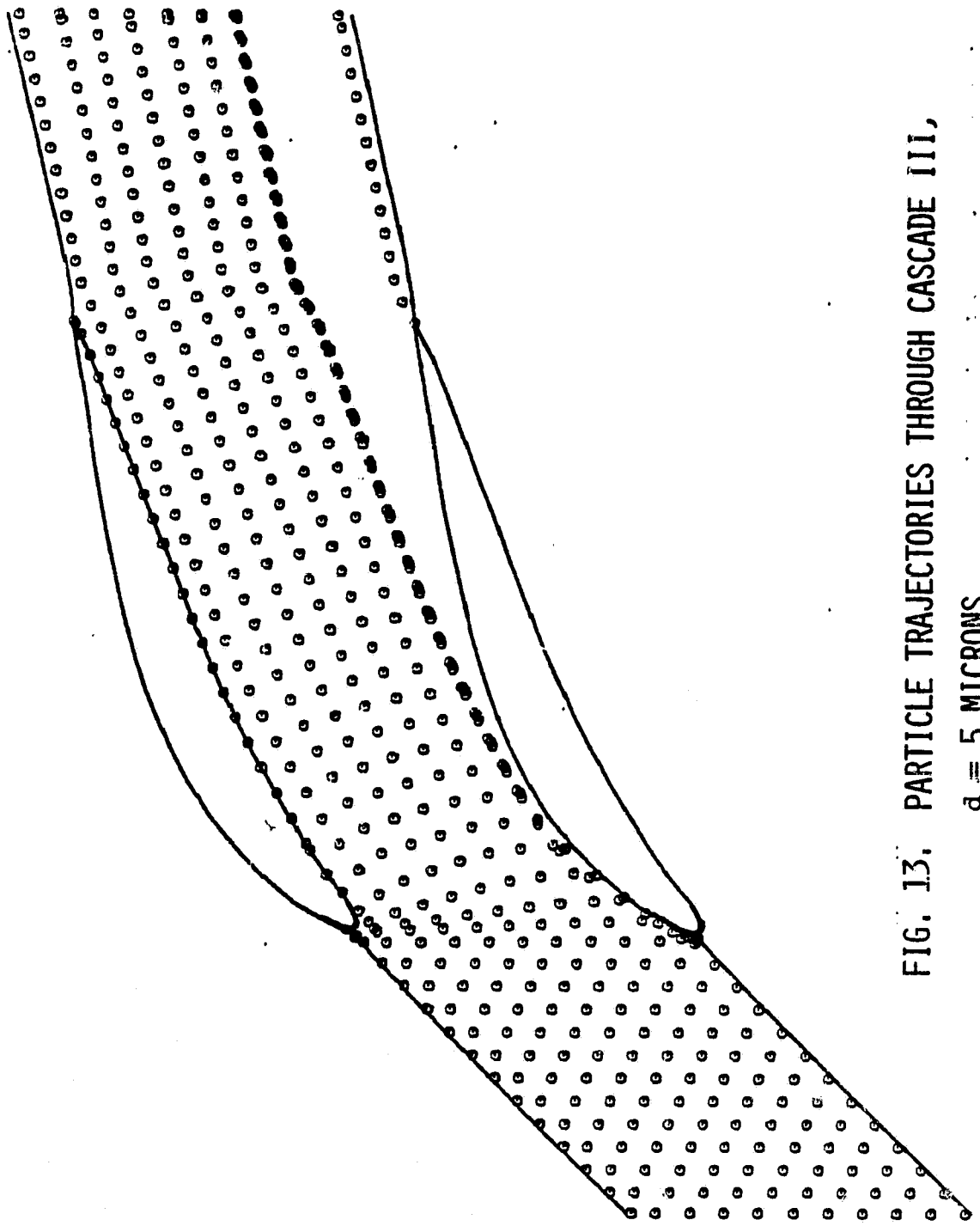

FIG. 13. PARTICLE TRAJECTORIES THROUGH CASCADE III, d_p = 5 MICRONS.

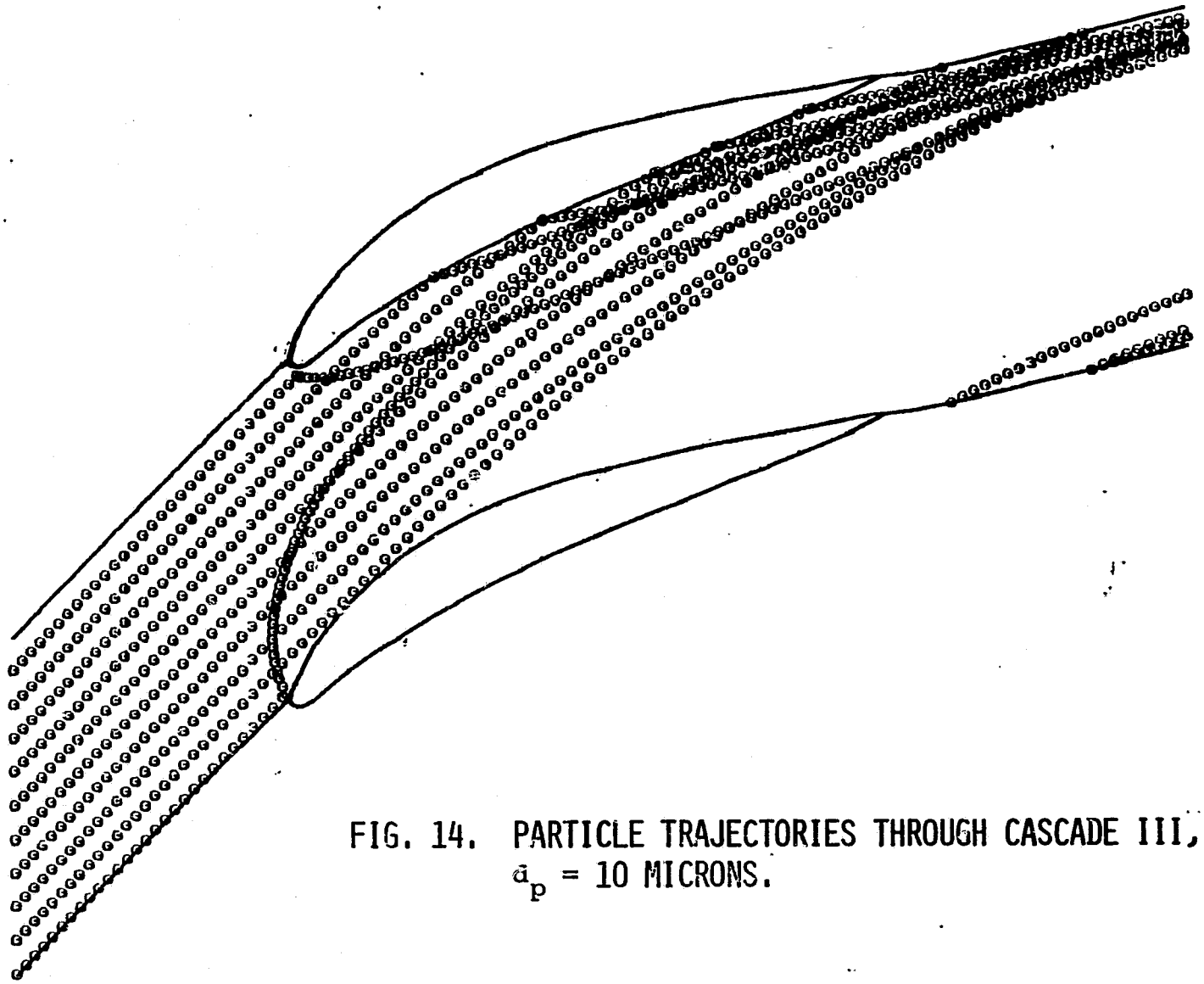

FIG. 14. PARTICLE TRAJECTORIES THROUGH CASCADE III, d_p = 10 MICRONS.

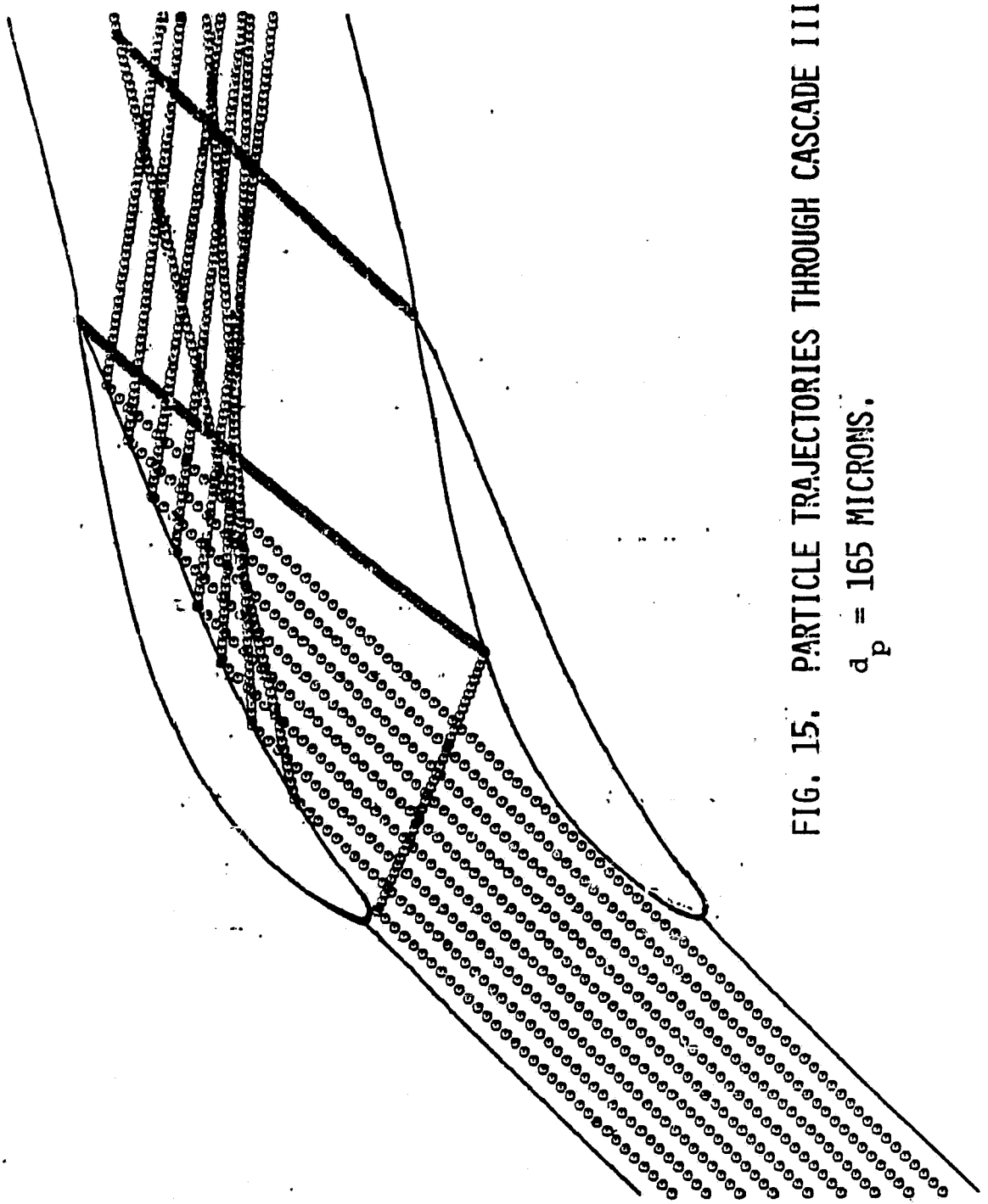

FIG. 15. PARTICLE TRAJECTORIES THROUGH CASCADE III, d_p = 165 MICRONS.

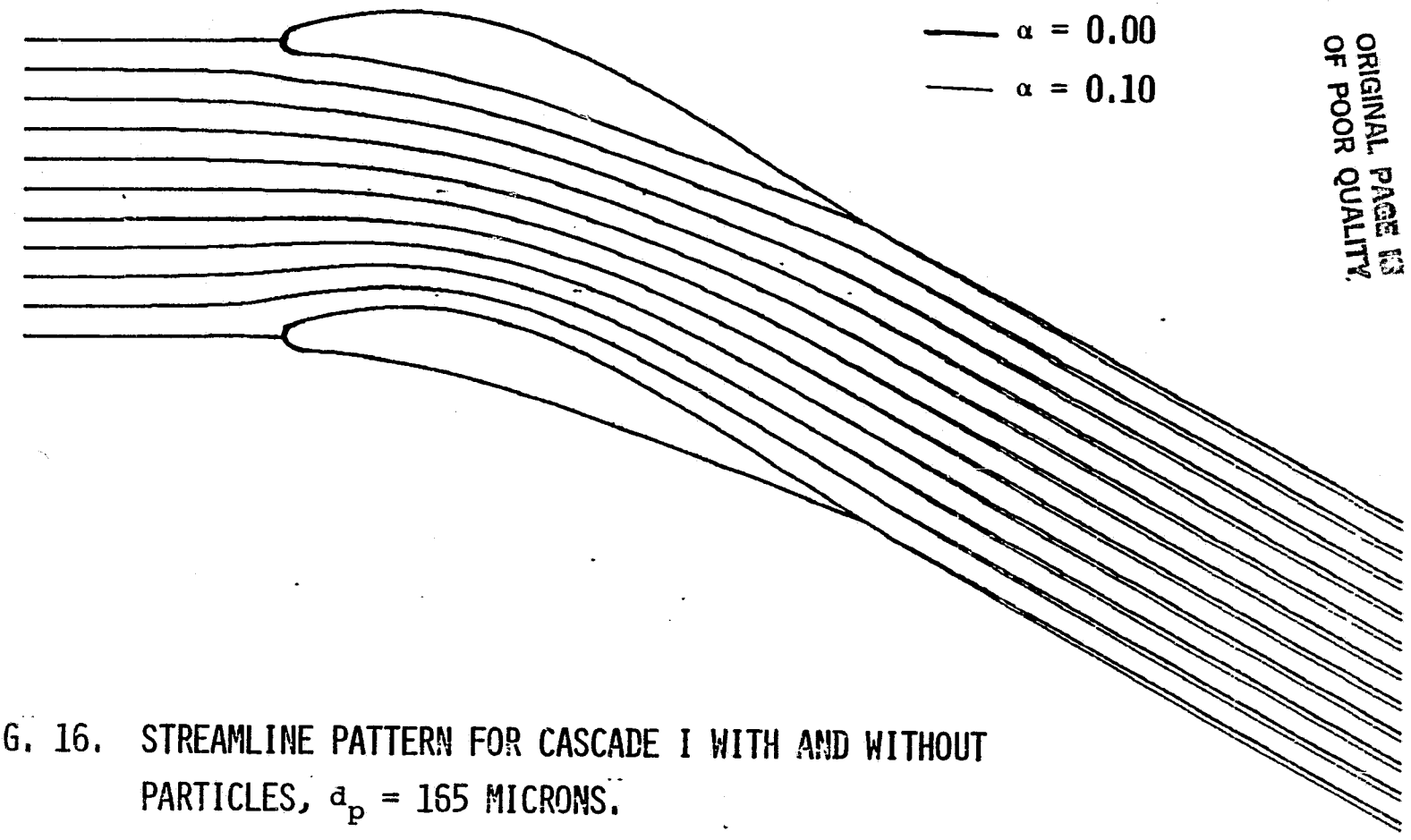

FIG. 16. STREAMLINE PATTERN FOR CASCADE I WITH AND WITHOUT PARTICLES, d_p = 165 MICRONS.

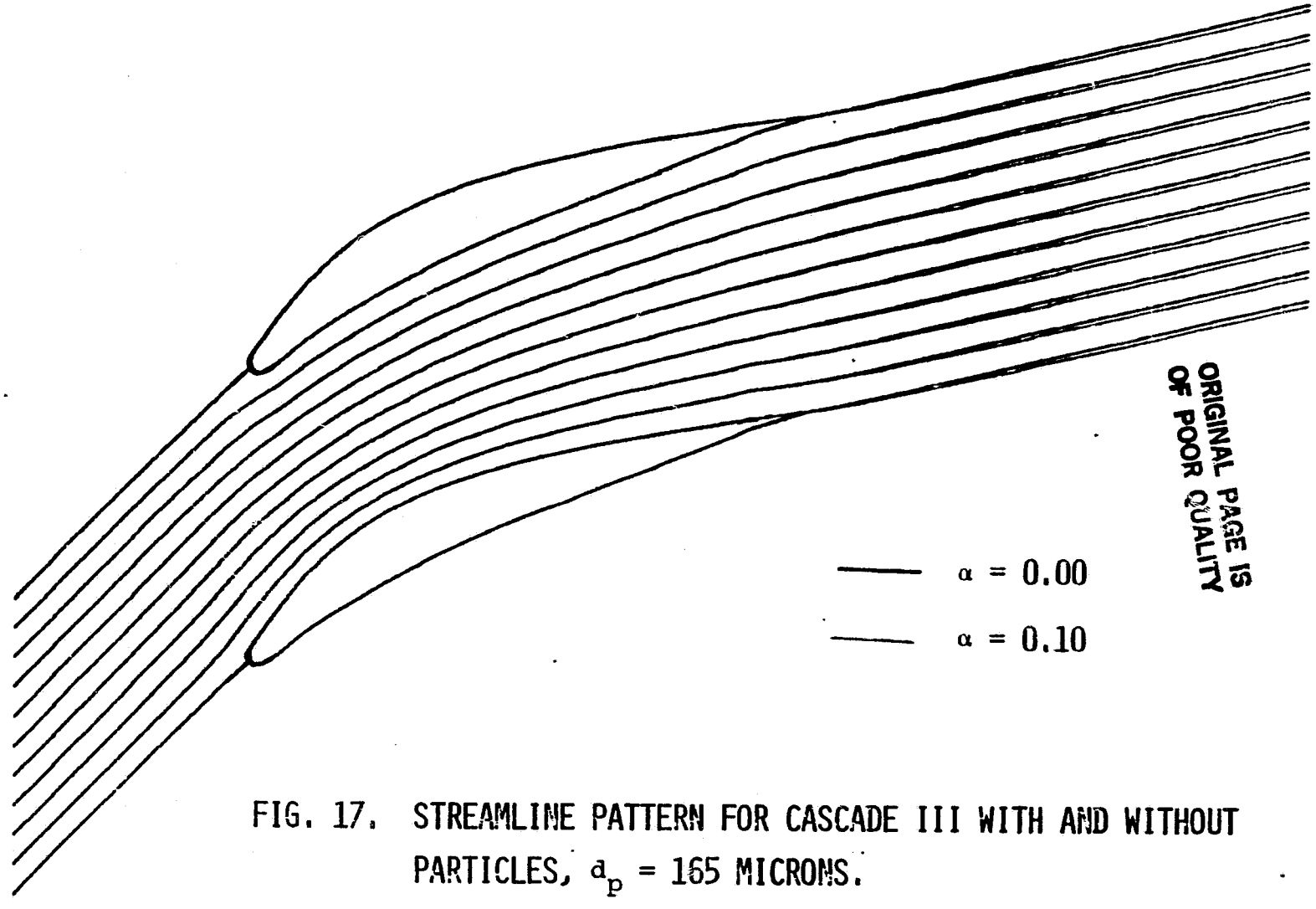

FIG. 17. STREAMLINE PATTERN FOR CASCADE III WITH AND WITHOUT PARTICLES, d_p = 165 MICRONS.

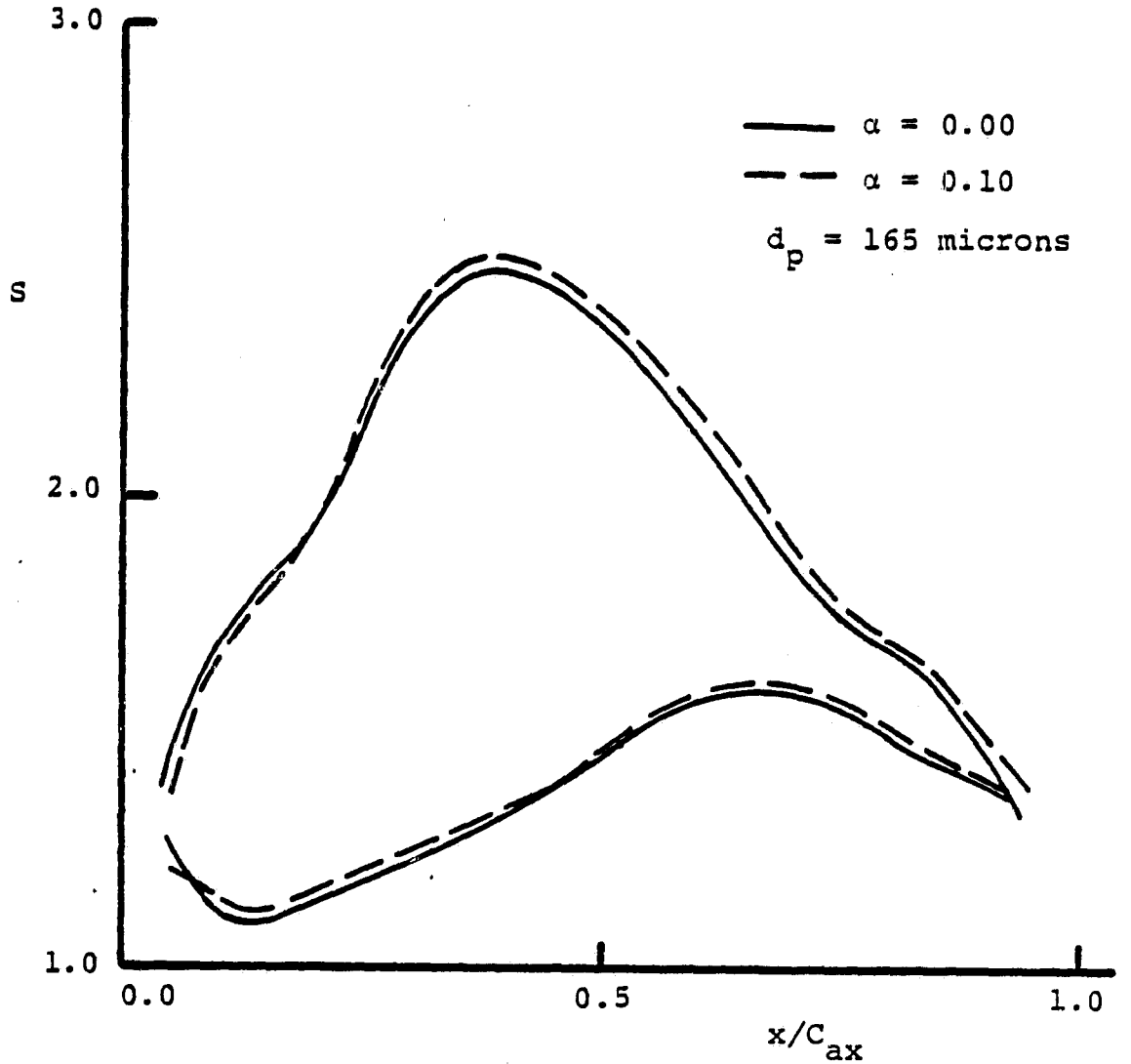

FIG. 18. COMPUTED PRESSURE DISTRIBUTION FOR CASCADE I FOR $\alpha = 0.0$ AND $\alpha = 0.10$.

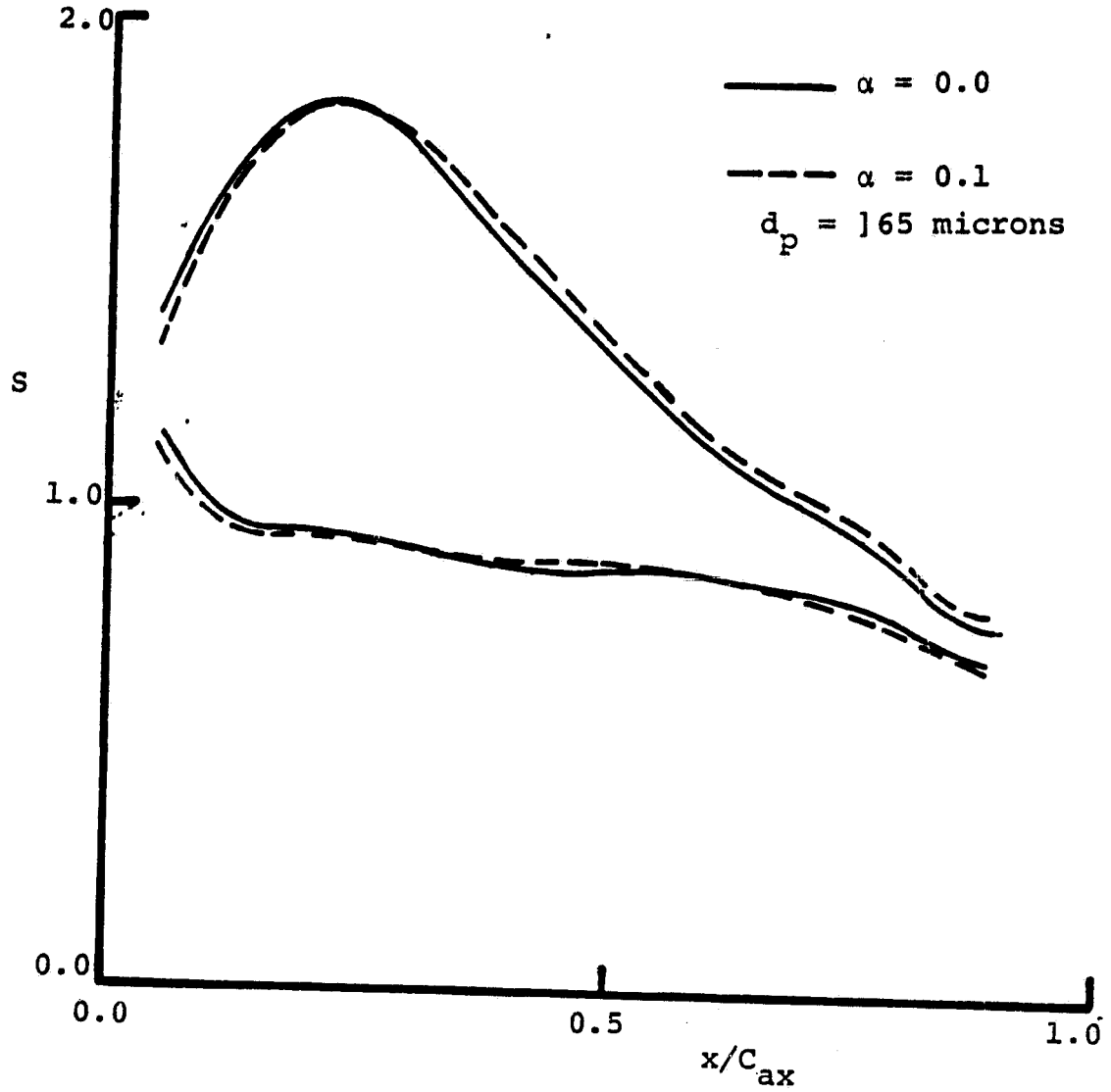

FIG. 19. COMPUTED PRESSURE DISTRIBUTION FOR CASCADE II FOR $\alpha = 0.0$ AND $\alpha = 0.10$.

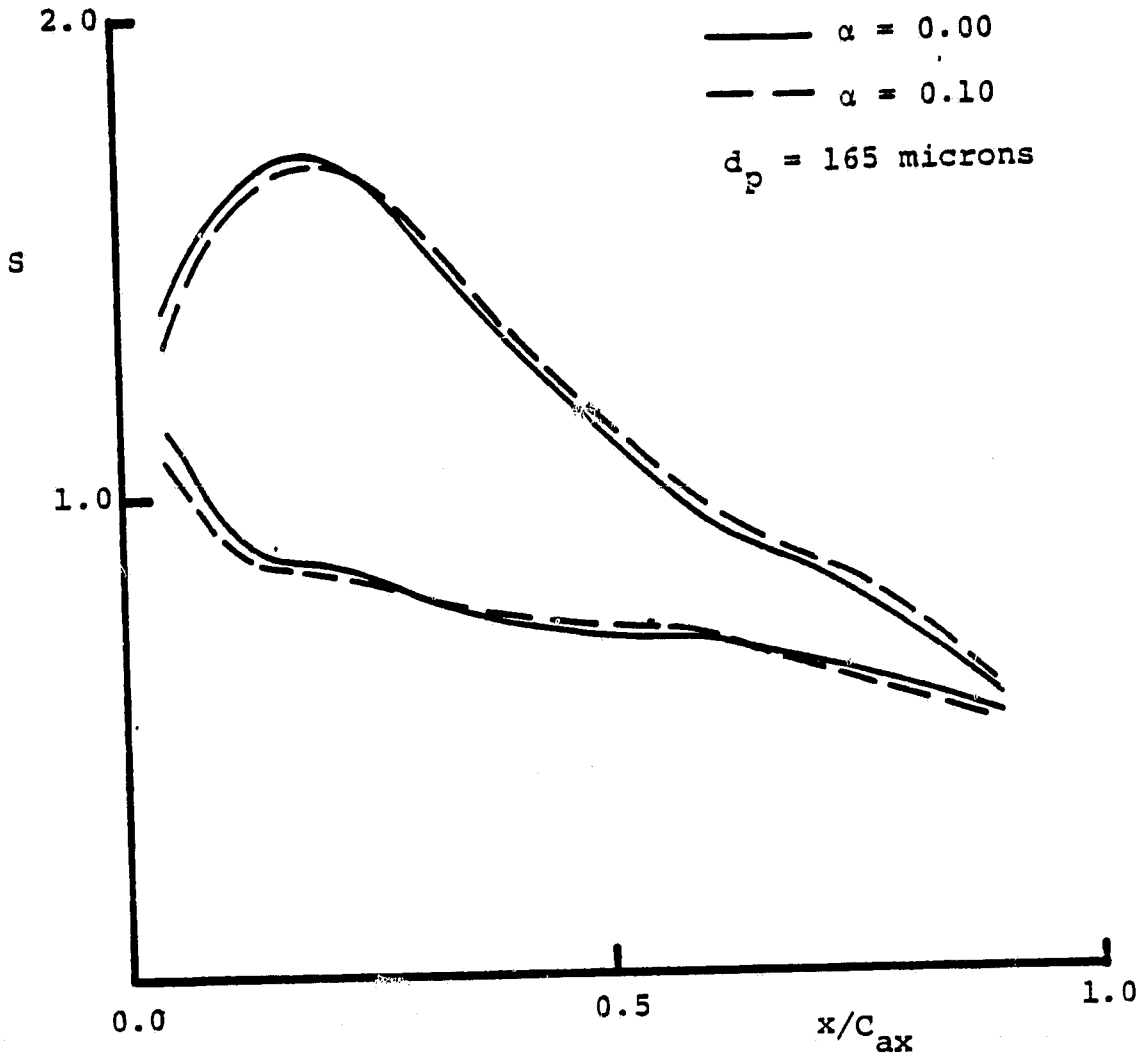

FIG. 20. COMPUTED PRESSURE DISTRIBUTION FOR CASCADE III, FOR $\alpha = 0.0$ AND $\alpha = 0.10$.

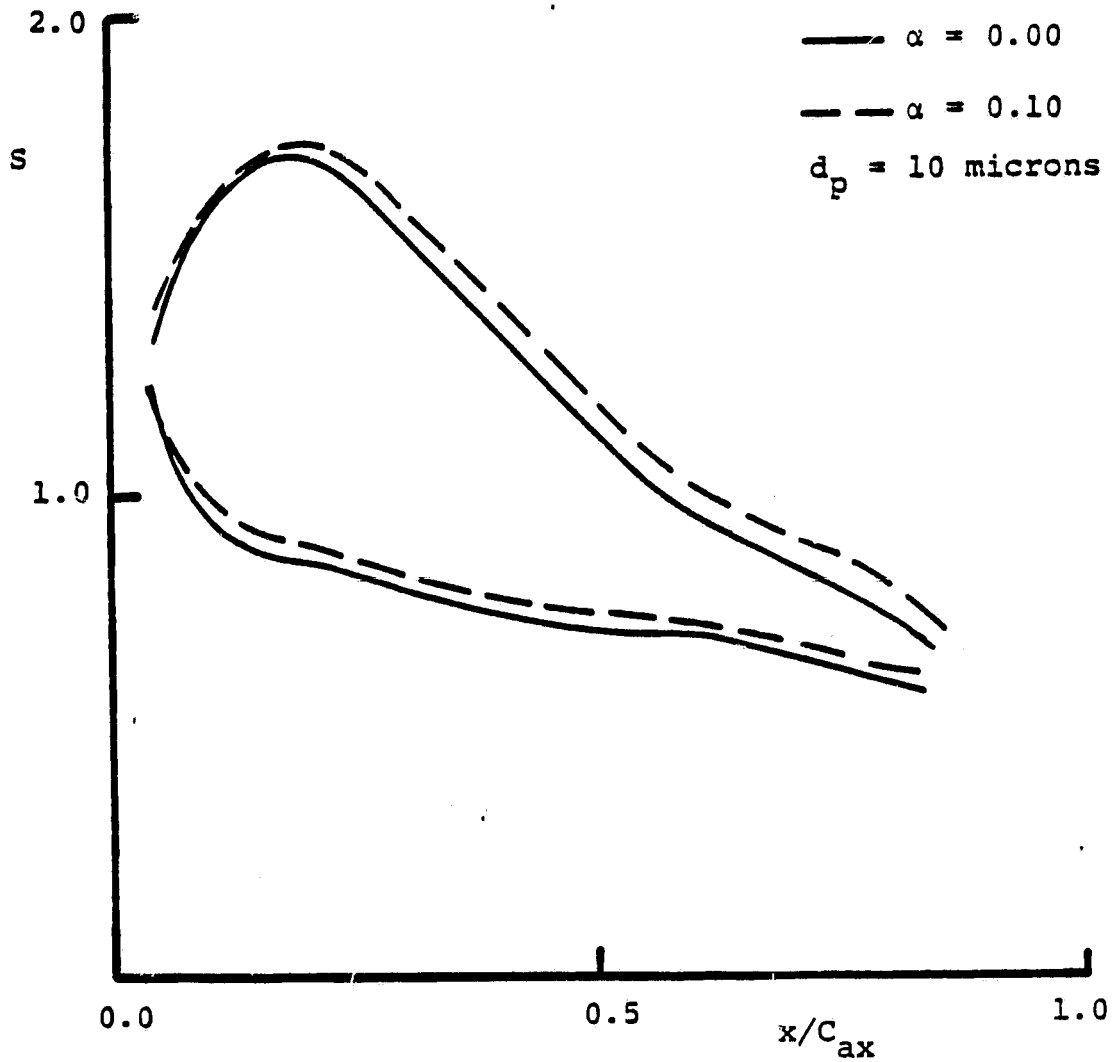

FIG. 21. COMPUTED PRESSURE DISTRIBUTION FOR CASCADE III, FOR $\alpha = 0.0$ AND $\alpha = 0.10$.

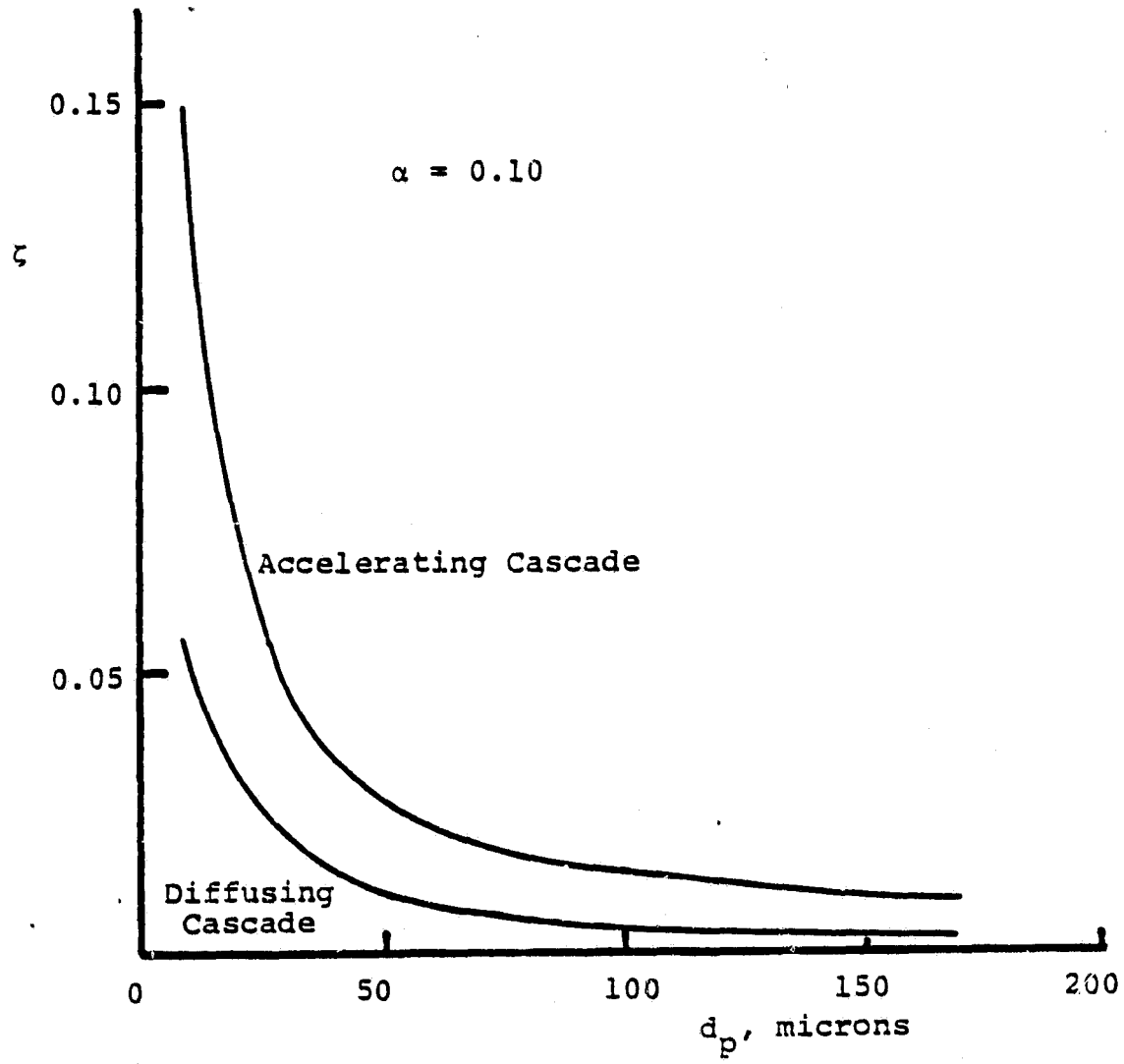

FIG. 22. COMPUTED EFFECT OF PARTICLE SIZE ON TOTAL PRESSURE LOSS COEFFICIENT.

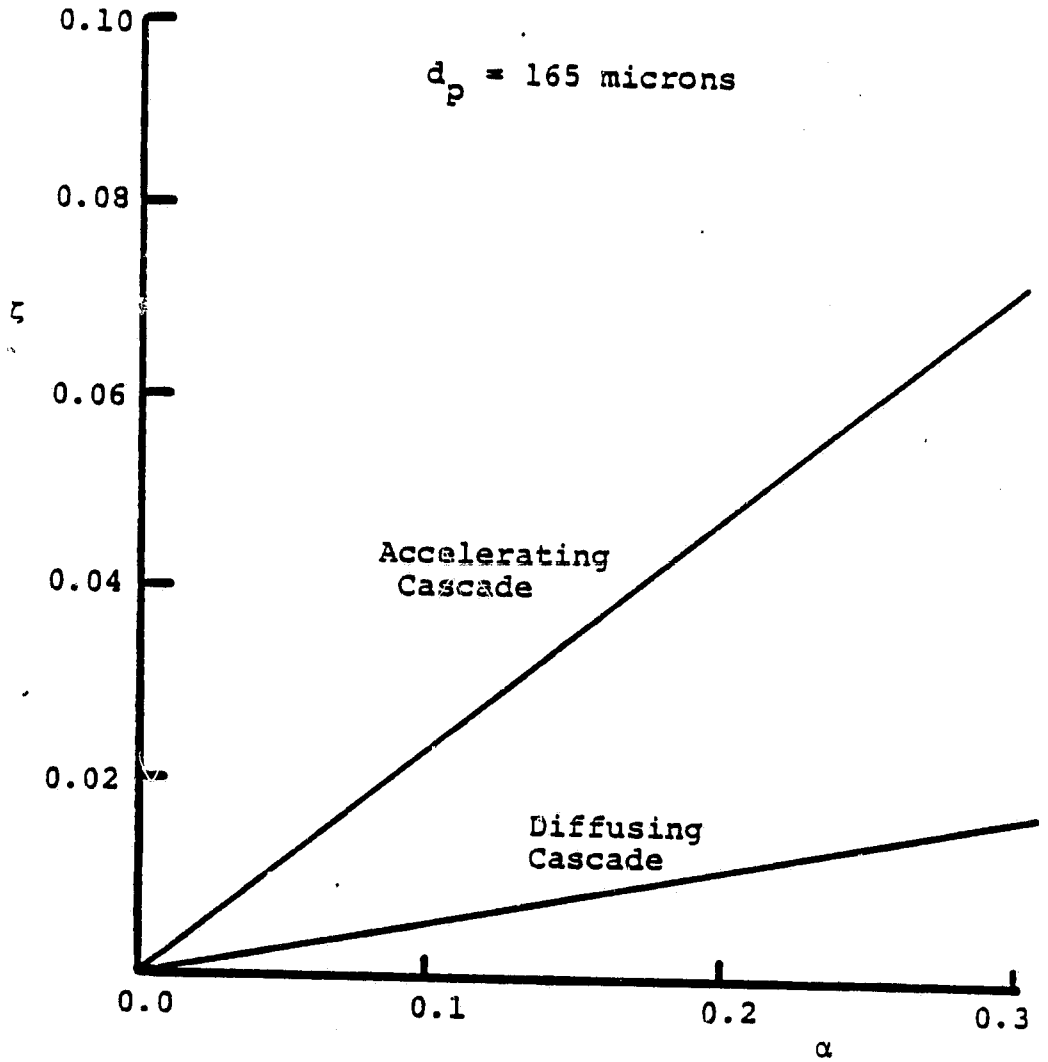

FIG. 23. COMPUTED EFFECT OF PARTICLE CONCENTRATION ON TOTAL PRESSURE LOSS COEFFICIENT.

APPENDIX A

The method of solution of the stream function-vorticity equations depends mainly on the choice of the coordinate system. A proper choice of such system simplifies the application of boundary conditions. The ξ coordinates were chosen as lines of constant x, which enables one to apply the periodicity boundary conditions for cascade flow. The η coordinates were chosen as any body fitted coordinate lines.

In the present problem, the vorticity generation mechanism is due to the interphase force gradients. In order to get a fairly smooth force gradient at all points, the grid system has to be fairly coarse. Since the error in the computed vorticity at the body surface can be large in a coarse mesh, it is preferrable not to use the vorticity at the body surface during the computation. This can be achieved by exploiting the transport properties of the vorticity equation (10). In the case that the lines of constant η are the same as the streamlines, the vorticity equation can be solved by marching along the streamlines. Since the gradient ψ_ξ is zero, the term $\omega_\eta \psi_\xi$ vanishes. However, one does not know the streamlines apriori. The other alternative is to neglect the term $\omega_\eta \psi_\xi$ in equation (10) and march along lines of constant η. The error in the computed vorticity can be minimized if the η coordinates are updated to the new streamline pattern at every iteration.

The advantages of this method are that the only information needed is the vorticity values at the inlet boundary and the

solution procedure does not use the vorticity at the blade surfaces.

Neglecting the term $\omega_\eta \psi_\xi$ on the left hand side of equation (10) results in

$$\omega_\xi \psi_\eta = \frac{1}{k\rho_g} [-F_{x_\eta} + F_{y_\xi} y_\eta - F_{y_\eta} y_\xi] \tag{A.1}$$

The stream function equation can be simplified to

$$A \frac{\partial \psi}{\partial \xi} + B \frac{\partial \psi}{\partial \eta} + C \frac{\partial^2 \psi}{\partial \eta^2} + D \frac{\partial^2 \psi}{\partial \xi^2} + E \frac{\partial^2 \psi}{\partial \xi \partial \eta} = - \frac{J\omega}{k} \tag{A.2}$$

where

$$A = \frac{\partial y_\eta}{\partial \xi} - \frac{\partial y_\xi}{\partial \eta} \quad , \qquad B = \frac{\partial y_\eta (1 + y_\xi^2)}{\partial \eta} - \frac{\partial y_\xi}{\partial \xi} \quad ,$$

$$C = y_\eta \quad , \qquad D = y_\eta (1 - y_\xi^2) \quad , \qquad E = -2. * y_\xi \tag{A.3}$$

Boundary Conditions

The boundary conditions for the above stream function equation (A.2) are (Fig. 1):

For both the upstream boundary (A-B) and downstream boundary (E-F), the inlet and exit angles β_1 and β_2 are specified as:

$$\tan \beta_1 = \left(\frac{v_g}{u_g}\right)_{\text{inlet}} = (y_\xi - y_\eta \psi_\xi / \psi_\eta)_{\text{inlet}} \tag{A.4}$$

$$\tan \beta_2 = \left(\frac{v_g}{u_g}\right)_{\text{exit}} = (y_\xi - y_\eta \psi_\xi / \psi_\eta)_{\text{exit}} \tag{A.5}$$

For the periodic boundaries (AH), (BC), (AF) and (DE):

$$\psi_{(BC)} = \psi_{(AH)} + 1.0$$

$$\psi_{(DE)} = \psi_{(GF)} + 1.0 \qquad \text{(A.6)}$$

Along the airfoil surfaces:

Suction Side (H-G)

$$\psi = 0.0 \qquad \text{(A.7)}$$

Pressure Side (C-D)

$$\psi = 1.0 \qquad \text{(A.8)}$$

Trailing Edge Condition

During the marching solution of the vorticity equation (A.1), one needs the information at the trailing edge vorticity. In potential flow, the vorticity at the trailing edge is zero. However, for the present case, where the total pressure is not uniform in the flow field, the trailing edge vorticity cannot be zero. The usual closure conditions applied for potential flow with uniform total pressure are that all the flow properties are continuous and subsequently, the velocity gradient normal to the trailing edge is zero, or that the pressure side and suction side velocities are equal at the trailing edge. In the present case, where the total pressure is not the same on either blade side, the flow requirements are that the mass flow and static pressure are continuous across the blade trailing edge. This implies that the velocity field across the trailing

edge is not continuous, consequently, the vorticity is not zero at the trailing edge. The vorticity at the trailing edge was computed as the sum of the blade suction and pressure side vorticities [9].

Finite Difference Scheme

Stream function equation:

The finite difference form of the stream function equation (A.2) was obtained using the nine point central differences of accuracy $0(\Delta\eta^2, \Delta\xi^2)$. Referring to Fig. (A.1) for any point i,j:

$$A_1 \psi_{i-1,j-1} + A_2 \psi_{i-1,j} + A_3 \psi_{i,j+1} + A_4 \psi_{i,j-1} + A_5 \psi_{i,j}$$

$$+ A_6 \psi_{i,j+1} + A_7 \psi_{i+1,j-1} + A_8 \psi_{i+1,j} + A_9 \psi_{i+1,j+1}$$

$$= \frac{J_{i,j}\omega_{i,j}}{k_{i,j}} \qquad (A.9)$$

where

$$A_1 = -\frac{E}{(4\Delta\eta\Delta\xi A_0)} \quad , \quad A_2 = (-\frac{A}{(2\Delta\xi)} + \frac{C}{(\Delta\xi^2)})/A_0 \quad ,$$

$$A_3 = -A_1 \quad , \quad A_4 = (-\frac{B}{(2\Delta\eta)} + \frac{D}{(\Delta\eta^2)})/A_0 \quad ,$$

$$A_5 = 1.0 \quad , \quad A_6 = (\frac{B}{(2\Delta\eta)} + \frac{D}{(\Delta\eta^2)})/A_0 \quad ,$$

$$A_7 = -A_1 \quad , \quad A_8 = (\frac{A}{(2\Delta\xi)} + \frac{C}{(\Delta\xi^2)})\,A_0 \quad ,$$

$$A_9 = A_1 \quad \text{and} \quad A_0 = 2(\frac{C}{\Delta\xi^2} + \frac{D}{\Delta\eta^2}) \quad .$$

and the constants A, B, C, D and E are the transformation parameters defined by equation (A.3) evaluated at point (i,j).

This gives raise to a system of n equations where n is the number of points at which ψ is to be evaluated:

$$[\bar{A}]\ [\psi] = [\bar{\omega}] \tag{A.10}$$

The above system of equations can be solved by any known methods. For the present purpose, they were solved by a banded matrix solver (Refs. [10, 11]).

Vorticity transport equation:

Considering equation (A.2), we can write it as

$$\frac{\omega_{i,j} - \omega_{i-1,j}}{\Delta\xi} = \frac{1}{k\ \rho_g\ \psi_{\eta_{i-\frac{1}{2},j}}} [-F_{x\eta_{i-\frac{1}{2},j}} + F_{y\xi_{i-\frac{1}{2},j}} * y_{\bar{\eta}_{i-\frac{1}{2},j}}$$

$$- F_{y\eta_{i-\frac{1}{2},j}} * y_{\xi_{i-\frac{1}{2},j}}] \tag{A.11}$$

which can be solved by marching along the lines of constant η (i.e. the streamlines)

$$\omega_{i,j} = \omega_{i-1,j} + k\ \frac{\Delta\xi}{\rho_g\ u_{i-\frac{1}{2},j}} [-F_{x\eta_{i-\frac{1}{2},j}} + F_{y\xi_{i-\frac{1}{2},j}} * y_{\eta_{i-\frac{1}{2},j}}$$

$$- F_{y\eta_{i-\frac{1}{2}}} * y_{\xi_{i-\frac{1}{2},j}} \tag{A.12}$$

Solution Procedure

The solution was started with an assumed pattern of streamlines satisfying the inlet and outlet flow angle requirements. The vorticity was assumed to be zero and the irrotational flow streamlines were found for 21 streamlines. This was followed by the computation of trajectories for 100 particles introduced at the inlet. The particles equation of motion was solved by time marching technique. The particle impact point was found by Newton-Raphson iteration method. This was followed by the computation of the force terms, which were assumed to be associated with the streamlines rather than the fixed spatial coordinate.

Once the force terms are computed, the vorticity is computed by marching along the η coordinates. This is followed by the stream function solution. Then the coordinates are updated and the process is repeated until the streamlines and the vorticity converge. This criteria was 0.01% relative error for the vorticity and 0.01% of the pitch for the streamlines. However, additional iterations were needed starting from the computation of the trajectories, since the force terms were associated with the streamlines rather than a fixed spatial point. The Flow Chart for the method of solution is given in Fig. A.2.

The pressure solution was obtained by integration of the momentum equation along η and ξ directions.

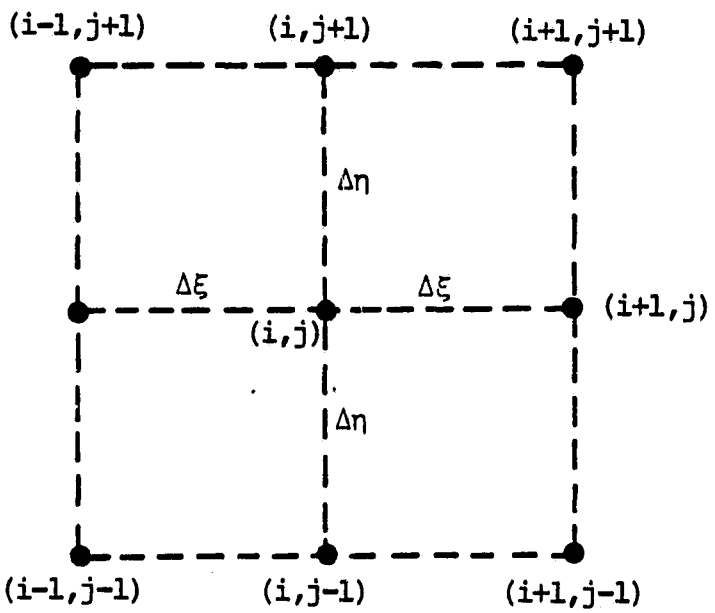

FIG. A.1. FINITE-DIFFERENCE NOMENCLATURE.

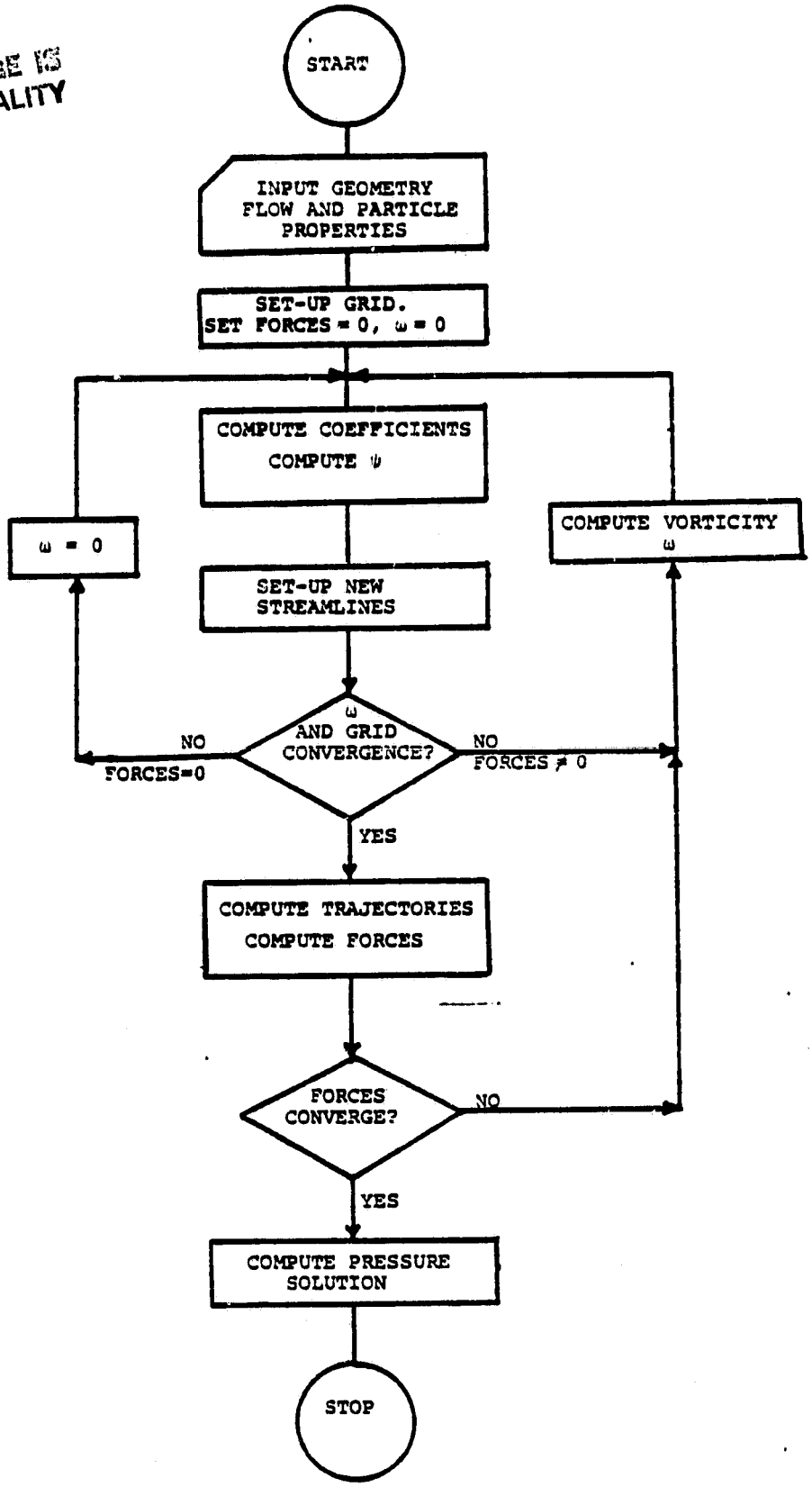

FIG. A2. FLOW CHART OF THE COMPUTER PROGRAM.